

The X17 boson and the $d(p, e^+e^-)^3\text{He}$ and $d(n, e^+e^-)^3\text{H}$ processes: a theoretical analysis

M. Viviani¹, E. Filandri^{2,1}, L. Girlanda^{3,4}, C. Gustavino⁵, A. Kievsky¹, and L.E. Marcucci^{2,1}

¹INFN-Pisa, I-56127, Pisa, Italy

²Department of Physics “E. Fermi”,
University of Pisa, I-56127 Pisa, Italy

³Department of Mathematics and Physics,
University of Salento, I-73100 Lecce, Italy

⁴INFN-Lecce, I-73100 Lecce, Italy

⁵INFN Sezione di Roma, 00185 Rome, Italy

The present work deals with the e^+e^- pair production in the $d(p, e^+e^-)^3\text{He}$ and $d(n, e^+e^-)^3\text{H}$ processes, in order to evidenitiate possible effects due to the exchange of a hypothetical low-mass boson, the so-called X17. These processes are studied for energies of the incident beams in the range 18-30 MeV, in order to have a sufficient energy to produce such a boson, whose mass is estimated to be around 17 MeV. We first analyze them as a purely electromagnetic processes, in the context of a state-of-the-art approach to nuclear strong-interaction dynamics and nuclear electromagnetic currents, derived from chiral effective field theory (χ EFT). Next, we examine how the exchange of a hypothetical low-mass boson would impact the cross sections for such processes. We consider several possibilities, that this boson is either a scalar, pseudoscalar, vector, or axial particle. The main aim of the study is to exploit the specular structure of the ^3He and ^3H nuclei to investigate the isospin dependency of the X17-nucleon interaction, as the alleged “proto-phobicity”.

I. INTRODUCTION

In the last years, there were claims [1–5] that an unknown particle (denoted as “X17”) had been observed in the processes $^7\text{Li}(p, e^+e^-)^8\text{Be}$, $^3\text{H}(p, e^+e^-)^4\text{He}$, and $^{11}\text{B}(p, e^+e^-)^{12}\text{C}$ at the ATOMKI experimental facility situated in Debrecen (Hungary). The ^8Be result has been confirmed very recently by another experiment performed at the VNU University of Science in Hanoi (Vietnam) [6]. These claims were based on a $\approx 7\sigma$ excess of events in the angular distribution of leptonic pairs produced in these reactions, which have a Q -value of about 20 MeV. The excess could be explained by positing the emission of an unknown boson with a mass of about 17 MeV decaying into e^+e^- pairs.

The possible existence of a new kind of low mass particle (at the MeV scale) is a problem of current and intense theoretical and experimental interest (see, for example, Ref. [7] and references therein). This interest is, in fact, part of a broader effort aimed at identifying dark matter (DM). The search for bosonic DM candidates had already started by several years, by attempting to establish the possible existence of additional forces (beyond gravity), mediated by these bosons [8] between DM and visible matter. To one such class of particles belongs the so-called “dark-photon”, namely a boson of mass M_X having the same quantum numbers as the photon, and interacting with a Standard Model (SM) fermion f with a coupling constant given by εq_f , where q_f is the fermion electric charge. Following several years of experimental searches, “exclusion plots” in the ε - M_X parameter space were produced, restricting more and more the allowed region [7, 9]. One of the most stringent limits was provided by the NA48/2 experiment [10].

The observation of the ^8Be , ^4He , and ^{12}C anomalies by the ATOMKI and VNU groups soon spurred several

theoretical studies. In Ref. [11], the possibility that the X17 could be a vector boson was investigated in detail. In order to circumvent the NA48/2 limit, it was conjectured that the X17 could be “proto-phobic”, namely that it would couple much more weakly to the proton than to the neutron [11]. Many other theoretical studies were published afterwards [12–28].

On the experimental side, there are several experiments (MEGII [29], DarkLight [30], SHiP [31], the “Montreal X-17 Project” [32], TREK/E36 [33], PADME [34], and others [7]) planning specifically to search for such a light boson. In addition, large collaborations, such as BelleII [35], NA64 [36], and others, are dedicating part of their efforts in an attempt to clarify this issue. Recently, the reaction $^3\text{He}(n, e^+e^-)^4\text{He}$ has been proposed as a possible new process where the presence of X17 can be observed and, eventually, its properties can be determined [37].

Other stringent experimental constraints on the possible magnitude of the X17 coupling constants with nucleons come from various pion-decay experiments (as the KTeV anomaly [38] and SINDRUM-I experiment [39]). See the analyses of Refs. [27, 28] for a comprehensive discussion. Most of the analyses performed so far are based on the hypothesis that the X17 production takes place as a two-step process: *i*) the formation of a specific resonance with well defined quantum numbers of the final nucleus; *ii*) the emission of the X17 in the transition from this resonant state to the ground state. However, the studies performed assuming a full dynamic initial scattering state [40, 41] have shown that the situation is not so simple, as the contribution of many resonances and even of the direct capture from P waves have to be taken into account. Therefore, we stress the necessity of studying processes where the nuclear dynamics is fully taken into account.

Here, we present a study of the $d(p, e^+ e^-)^3\text{He}$ and $d(n, e^+ e^-)^3\text{H}$ reactions. The advantage of studying these processes is that for them it is possible to perform accurate *ab initio* calculations to describe bound- and continuum-states. We use the hyperspherical-harmonics (HH) method to determine them [42, 43], by taking fully into account the three-body dynamics. The employed nuclear Hamiltonians are very accurate. First of all we have employed the phenomenological Argonne v_{18} (AV18) [44] two-nucleon ($2N$) and the Urbana IX (UIX) [45] three-nucleon ($3N$) interaction. This interaction will be denoted hereafter as AV18UIX. Furthermore, we have also considered the Norfolk V_{Ia} 2N interaction [46, 47] plus the 3N force [48] derived within the framework of chiral effective field theory (χ EFT). This interaction will be denoted in the following as NVIa3N. To perform this study, we need accurate accompanying electromagnetic (EM) currents, as well. We have used those derived from the χ EFT study of Refs. [49–53]. The LECs entering these EM currents have been fixed by reproducing the trinucleon magnetic moments for both AV18UIX and NVIa3N interactions.

Regarding the X17 interaction, following Ref. [40], we consider the general case of a Yukawa-like interaction between this boson and a SM fermion of species f (specifically, u and d quarks, and electrons) with the coupling constant expressed as $\varepsilon_f e$, where $e > 0$ is the unit electric charge. The X17 boson must decay promptly in $e^+ e^-$ pairs for these to be detected inside the experimental setup. This observation actually introduces a *lower limit* to the possible values of ε_e , the X17-electron coupling constant. These limits are also established by various electron beam-dump experiments (see, for example, Ref. [54] and references therein). For $M_X \approx 17$ MeV, the most stringent lower bound, $|\varepsilon_e| > 2 \times 10^{-4}$, comes from the SLAC E141 experiment [55], while the upper bound $|\varepsilon_e| < 2 \times 10^{-3}$ has been set by the KLOE-2 experiment [56]. However, we will show that in the considered nuclear processes there is no sensitivity to ε_e . In the following, we will assume $\varepsilon_e = 10^{-3}$ and study how the angular distribution of the two leptons is affected by the values of the spin and parity of the X17 boson.

The Lagrangian interaction terms with hadrons (specifically, nucleons and pions) are obtained by placing the X17 as an external source in the QCD Lagrangian [57–59]. Considering only interactions invariant under parity, charge conjugation and time reversal, we examine four possible X17-quarks interaction types: scalar, pseudoscalar, vector, and axial. These Lagrangian terms will depend on a number of low-energy constants (LECs), which take into account the hadron dynamics induced by QCD. Many of these LECs are known as they also enter various nuclear processes, as for example nucleon-nucleon scattering, pion decay, etc. Therefore, they can be extracted from experimental data. Then, using the quark-X17 coupling constants given in Ref. [40], as determined in order to reproduce the $p(^3\text{H}, e^+ e^-)^4\text{He}$ experimental data of Ref. [2], we will be able to pre-

dict the contribution of an X17 (of mass 17 MeV) in the $d(p, e^+ e^-)^3\text{He}$ and $d(n, e^+ e^-)^3\text{H}$ reactions. This can be done for the four considered X17-quarks interaction types.

Assuming standard physics, the excited ^3H and ^3He nuclei have no resonant levels and decay to the ground state mainly with the emission of a single photon via an electric dipole transition. The production of the X17 is possible only above a well definite energy of the beam, $E_p > 17.3$ MeV ($E_n > 16.1$ MeV). Under such thresholds, no peak should be observed. Also the position of peak in the $e^+ - e^-$ angular distribution is strictly connected to the beam energy and X17 mass value. Therefore, having the possibility to vary the beam energy, let us say in the 18 – 30 MeV range, one could put a severe constraint on the existence and mass of X17 (and whether it is either a scalar, vector, pseudoscalar, or axial particle). Moreover, as stated before, the possibility to compare the $d(p, e^+ e^-)^3\text{He}$ and $d(n, e^+ e^-)^3\text{H}$ experimental cross sections could give important information regarding the isospin dependence of the X17 interaction with quarks.

The work described in this contribution is based on the study presented in Ref. [40]. In Sec. II, a brief description of the theoretical formalism is given. Then, in Sec. III the results of the calculations are reported and discussed. Finally, in the last section, the perspectives of this study are given.

II. THEORETICAL ANALYSIS

A. The interaction Lagrangian

In this work, the interaction Lagrangian density at energy scale $\Lambda_H \sim 1$ GeV is considered to be

$$\mathcal{L}_X^c(x) = e \varepsilon_e^c \bar{e}(x) \Gamma^c e(x) X_c(x) + \mathcal{L}_{q,X}^c(x) , \quad (1)$$

where $e(x)$ is the electron field and $X_c(x)$ the X17 field (see below). In the following, we will consider four cases: $c = S, P, V, A$ for a scalar, pseudoscalar, vector, or axial boson. Correspondingly,

$$\Gamma^{c=S,P,V,A} = 1, i \gamma^5, \gamma^\mu, \gamma^\mu \gamma^5 . \quad (2)$$

The various coupling constants will be always written in units of the electric charge $e > 0$ ($e^2 = 4\pi\alpha$, where $\alpha \approx 1/137$ is the fine structure constant).

The part $\mathcal{L}_{q,X}^c(x)$ describes the interaction of the X17 with quarks. For a scalar (S) or pseudoscalar (P) X17 boson, we take as

$$\mathcal{L}_{q,X}^c(x) = e \frac{1}{\Lambda} \sum_{f=u,d,\dots} m_f \varepsilon_f^c \bar{f}(x) \Gamma^c f(x) X_c(x) , \quad c = S, P , \quad (3)$$

where $f(x)$ is the field of the quark of flavour f , Λ an unknown high-energy mass scale, and we have introduced explicitly the quark masses m_f , $f = u, d, \dots$, in order

to have renormalization-scale invariant amplitudes. In Eq. (3), the sum runs over the lightest fermions of the SM. Reducing to the case of only u and d quarks, it is possible to rewrite this Lagrangian in terms of the isodoublet quark fields $q(x)$, defined as

$$q(x) = \begin{bmatrix} u(x) \\ d(x) \end{bmatrix}, \quad (4)$$

in the following way

$$\mathcal{L}_{q,X}^c(x) = e \frac{m_q}{\Lambda_S} \bar{q}(x) (\varepsilon_0^c + \varepsilon_z^c \tau_3) \Gamma^c q(x) X_c(x), \quad c = S, P, \quad (5)$$

where τ_3 is a Pauli matrix, m_q is the average light-quark mass, and we have introduced the coupling constants (again $c = S, P$)

$$\varepsilon_0^c = \frac{\Lambda_S}{\Lambda} \frac{m_u \varepsilon_u^c + m_d \varepsilon_d^c}{2 m_q}, \quad (6)$$

$$\varepsilon_z^c = \frac{\Lambda_S}{\Lambda} \frac{m_u \varepsilon_u^c - m_d \varepsilon_d^c}{2 m_q}, \quad (7)$$

and a new scale Λ_S which we set (arbitrarily) at 1 GeV.

For a vector (V) or axial (A) X17, the Lagrangian is taken as

$$\mathcal{L}_{q,X}^c(x) = e \sum_{f=u,d,\dots} \varepsilon_f^c \bar{f}(x) \Gamma^c f(x) X_c(x), \quad c = V, A. \quad (8)$$

Therefore, in case of only two quarks, it can be rewritten as

$$\mathcal{L}_{q,X}^c(x) = e \bar{q}(x) (\varepsilon_0^c + \varepsilon_z^c \tau_3) \Gamma^c q(x) X_c(x), \quad (9)$$

where we have introduced the coupling constants

$$\varepsilon_0^c = \frac{\varepsilon_u^c + \varepsilon_d^c}{2}, \quad (10)$$

$$\varepsilon_z^c = \frac{\varepsilon_u^c - \varepsilon_d^c}{2}. \quad (11)$$

Note that a proto-phobic X17 is defined to have $2\varepsilon_u^c + \varepsilon_d^c = 0$, or equivalently

$$3\varepsilon_0^c + \varepsilon_z^c = 0. \quad (12)$$

Finally, for the $c=S, P$ cases, the X17 field is a scalar field, $X_c(x) = X(x)$. On the other hand, for the $c=V, A$ cases, the X17 field is a vector field, $X_c(x) = X_\mu(x)$.

Starting from these Lagrangians, it is possible to derive nucleon-X17 interaction Lagrangian densities in the framework of χ EFT. By retaining only leading-order contributions (and selected subleading ones in the vector and pseudoscalar cases), one obtains (for a detailed derivation, see Ref. [40])

$$\mathcal{L}_X^S(x) = e \bar{N}(x) [\eta_0^S + \eta_z^S \tau_3] N(x) X(x), \quad (13)$$

$$\mathcal{L}_X^P(x) = e \eta_z^P \pi_3(x) X(x) + e \eta_0^P \bar{N}(x) i \gamma^5 N(x) X(x), \quad (14)$$

$$\begin{aligned} \mathcal{L}_X^V(x) = e \bar{N}(x) [\eta_0^V + \eta_z^V \tau_3] \gamma^\mu N(x) X_\mu(x) \\ + \frac{e}{4m_N} \bar{N}(x) [\kappa_0 \eta_0^V + \kappa_z \eta_z^V \tau_3] \sigma^{\mu\nu} N(x) F_{\mu\nu}^X(x), \end{aligned} \quad (15)$$

$$\mathcal{L}_X^A(x) = e \bar{N}(x) [\eta_0^A + \eta_z^A \tau_3] \gamma^\mu \gamma^5 N(x) X_\mu(x), \quad (16)$$

where m_N is the nucleon mass, $N(x)$ is the iso-doublet of nucleon fields, $\pi_3(x)$ is the third component of the triplet of pion fields, and $F_{\mu\nu}^X(x) = \partial_\mu X_\nu(x) - \partial_\nu X_\mu(x)$ is the X17 field tensor. The hadron-X17 coupling constants η_0^c and η_z^c are linear combinations of the quark-X17 coupling constants ε_u^c and ε_d^c [40]

$$\begin{aligned} \eta_0^S &= -\frac{4m_\pi^2 c_1}{\Lambda_S} \varepsilon_0^S, \\ \eta_z^S &= -\frac{2m_\pi^2 c_5}{\Lambda_S} \varepsilon_z^S, \\ \eta_0^P &= 2 \frac{m_\pi^2 m_N (d_{18} + 2 d_{19})}{\Lambda_S} \varepsilon_0^P, \\ \eta_z^P &= \frac{m_\pi^2 f_\pi}{\Lambda_S} \varepsilon_z^P, \\ \eta_0^V &= 3 \varepsilon_0^V, \\ \eta_z^V &= \varepsilon_z^V, \\ \eta_0^A &= (3F - D) \varepsilon_0^A, \\ \eta_z^A &= (F + D) \varepsilon_z^A, \end{aligned} \quad (17)$$

where c_1, c_5, F , etc., are LECs entering the nuclear chiral Lagrangian. In the vector case, we have included also the subleading term proportional to $F_{\mu\nu}^X$ and where

$$\kappa_0 = \kappa_p + \kappa_n, \quad \kappa_z = \kappa_p - \kappa_n, \quad (18)$$

κ_p and κ_n being the anomalous magnetic moments of the proton and neutron, respectively. In the pseudoscalar case, the interaction at leading order in the power counting originates from the direct coupling of the X17 to the pion. However, since the associated coupling constant is expected to be suppressed [19, 20], we have also considered an isoscalar coupling of the X17 to the nucleon, even though it is subleading, at least nominally, in the χ EFT power counting relative to the isovector one. As per the axial case, the leading order $\mathcal{L}_X^A(x)$ contains an additional term of the form $\partial^\mu \pi_3(x) X_\mu(x)$, which we have dropped. In fact, this term leads to a X17-nucleon current proportional to q^μ/m_π^2 (for low momentum transfers) which, when contracted with the lepton axial current, produces a contribution proportional to $(m_e/m_\pi)^2$, and hence negligible when compared to that resulting from the X17 direct coupling to the nucleon.

The X17-induced nuclear current by each of the (leading order) Lagrangians in Eqs. (13)–(16) can be easily calculated, for example, in time-ordered perturbation theory. By retaining the leading-order terms in the chiral and non-relativistic expansion of the various amplitudes,

the nuclear current J_X^c are expressed as

$$J_X^S = \eta_0^S \rho^{S+} + \eta_z^S \rho^{S-}, \quad (19)$$

$$J_X^P = \frac{g_A}{2f_\pi} \eta_z^P \frac{q}{q^2 + m_\pi^2} \rho^{P-} + \eta_0^P \frac{q}{2m_N} \rho^{P+}, \quad (20)$$

$$\rho_X^V = \eta_0^V \rho^{V+} + \eta_z^V \rho^{V-}, \quad (21)$$

$$J_X^V = \eta_0^V \left(\mathbf{j}^{V+} + \kappa_0 \bar{\mathbf{j}}^{V+} \right) + \eta_z^V \left(\mathbf{j}^{V-} + \kappa_z \bar{\mathbf{j}}^{V-} \right) \quad (22)$$

$$\rho_X^A = \eta_0^A \rho^{A+} + \eta_z^V \rho^{A-}, \quad (23)$$

$$J_X^A = \eta_0^A \mathbf{j}^{A+} + \eta_z^A \bar{\mathbf{j}}^{A-}, \quad (24)$$

where in the $c = V, A$ case the current has both a time (denoted as ρ_X^c) and a space (denoted as J_X^c) component. The nuclear currents above have been written in terms of the following single-particle “basic” adimensional operators:

$$\rho^{S\lambda}(\mathbf{q}) = \sum_{i=1}^A e^{i\mathbf{q}\cdot\mathbf{r}_i} P_i^\lambda, \quad (25)$$

$$\rho^{P\lambda}(\mathbf{q}) = \sum_{i=1}^A e^{i\mathbf{q}\cdot\mathbf{r}_i} i \hat{\mathbf{q}} \cdot \boldsymbol{\sigma}_i P_i^\lambda, \quad (26)$$

$$\rho^{A\lambda}(\mathbf{q}) = \sum_{i=1}^A \frac{1}{2m_N} [e^{i\mathbf{q}\cdot\mathbf{r}_i}, \mathbf{p}_i \cdot \boldsymbol{\sigma}_i]_+ P_i^\lambda, \quad (27)$$

$$\mathbf{j}^{V\lambda}(\mathbf{q}) = \sum_{i=1}^A \frac{1}{2m_N} [e^{i\mathbf{q}\cdot\mathbf{r}_i}, \mathbf{p}_i]_+ P_i^\lambda, \quad (28)$$

$$\bar{\mathbf{j}}^{V\lambda}(\mathbf{q}) = \sum_{i=1}^A \frac{i}{2m_N} e^{i\mathbf{q}\cdot\mathbf{r}_i} \mathbf{q} \times \boldsymbol{\sigma}_i P_i^\lambda, \quad (29)$$

$$\mathbf{j}^{A\lambda}(\mathbf{q}) = \sum_{i=1}^A e^{i\mathbf{q}\cdot\mathbf{r}_i} \boldsymbol{\sigma}_i P_i^\lambda, \quad (30)$$

where $\lambda = \pm$ with $P_i^+ = 1$ and $P_i^- = \tau_{i,3}$, \mathbf{p}_i is the momentum operator, and $[\dots]_+$ denotes the anticommutator.

Starting from the expressions above, at first order in perturbation theory, the amplitude for the emission of an e^+e^- pair between nuclear initial and final states is written in general as

$$T_{fi} = T_{fi}^{EM} + T_{fi}^{cX}, \quad (31)$$

where T_{fi}^{EM} is the one-photon-exchange amplitude written as

$$T_{fi}^{EM} = 4\pi\alpha \frac{(\bar{u}_- \gamma_\mu v_+) j_{EM}^\mu}{q^\mu q_\mu}, \quad (32)$$

$$j_{EM}^\mu = \langle \Phi_{m_3} | J_{EM}^{\mu\dagger} | \Psi_{m_2, m_1} \rangle, \quad (33)$$

where J_{EM}^μ is the nuclear EM current operator. Above, α is the fine structure constant, q^μ is the four-momentum transfer defined as the sum of the outgoing-lepton four momenta, and u_- and v_+ are, respectively, the electron and positron spinors. Moreover, Ψ_{m_2, m_1} is the initial

wave function describing the $N + d$ scattering state (see below), while Φ_{m_3} is the trinucleon ground state wave function of spin projection m_3 .

The term T_{fi}^{cX} is the amplitude with the exchange of an unknown boson X of type $c = S, P, V, A$, namely

$$T_{fi}^{cX} = 4\pi\alpha \frac{\varepsilon_e (\bar{u}_- \Gamma_c v_+) j_X^c}{q^\mu q_\mu - M_X^2}, \quad (34)$$

$$j_X^c = \langle \Phi_{m_3} | J_X^{c\dagger} | \Psi_{m_2, m_1} \rangle, \quad (35)$$

where M_X is the mass of the X particle, and j_X^c represents the matrix element of the X -induced nuclear current $J_X^{c\dagger}$ given in Eqs. (19)–(24), which depends on the X -hadron coupling constants η_0^c and η_z^c . Note that in the case $c = V, A$, such an operator is a four-vector.

B. $N - d$ wave functions and kinematics of the reactions

In the laboratory frame, the initial state consists of an incoming proton or neutron of momentum \mathbf{p} and spin projection m_1 , and a bound deuteron in spin state m_2 at rest. Its wave function Ψ_{m_2, m_1} is such that, in the asymptotic region of large separation \mathbf{y}_ℓ between the isolated nucleon (particle ℓ) and the deuteron (particles ij), it reduces to

$$\Psi_{m_2, m_1}(\mathbf{p}) \longrightarrow \frac{1}{\sqrt{3}} \sum_{\ell=1}^3 \phi_{m_2}(ij) \chi_{m_1}(\ell) \Phi_{\mathbf{p}}(\mathbf{y}_\ell), \quad (36)$$

where $\Phi_{\mathbf{p}}(\mathbf{y}_\ell)$ is either a Coulomb distorted wave or simply the plane wave $e^{i\mathbf{p}\cdot\mathbf{y}_\ell}$ depending on whether we are dealing with the $p + d$ or $n + d$ state (ϕ_{m_2} is the deuteron bound state wave function). The final state consists of the lepton pair—with the e^- having momentum (energy) \mathbf{k} (ϵ) and spin s , and the e^+ having momentum (energy) \mathbf{k}' (ϵ') and spin s' —and the trinucleon bound state recoiling with momentum $\mathbf{p} - \mathbf{k} - \mathbf{k}'$. We define hereafter $\mathbf{q} = \mathbf{k} + \mathbf{k}'$ and $\omega = \epsilon + \epsilon'$. Therefore, $q^\mu q_\mu \equiv Q^2 = \omega^2 - \mathbf{q}^2$. Energy conservation requires

$$\epsilon + \epsilon' + \frac{(\mathbf{p} - \mathbf{k} - \mathbf{k}')^2}{2M_3} = T_N + B_3 - B_2, \quad (37)$$

where M_3 is the rest mass of the trinucleon ground state (either ${}^3\text{He}$ or ${}^3\text{H}$) and B_3 and B_2 are the binding energies of, respectively, the bound three-nucleon cluster and the deuteron. Above, $T_N \equiv p^2/2m_N$ is the (laboratory) kinetic energy of the incident nucleon. Eq. (37) can be rewritten as

$$\epsilon + \epsilon' = E_0 - \frac{q^2 - 2\mathbf{p} \cdot \mathbf{q}}{2M_3}, \quad (38)$$

$$E_0 = T_N \left(1 - \frac{m_N}{M_3} \right) + B_3 - B_2. \quad (39)$$

Note that in good approximation $(1 - m_N/M_3) = 2/3$ and that $\epsilon + \epsilon' \approx E_0$.

The X17 is produced when $Q^2 \approx M_X^2$. For this reaction $B_3 - B_2 \approx 5$ MeV, hence the X17 could be produced only when $T_p \geq T_p^{min}$. To find the value of T_p^{min} , it is convenient to consider the reaction in the center-of-mass (CM) system. At the threshold energy, the X17 and the trinucleon are produced at rest. The energy conservation in this case reads

$$T_{(CM)}^{min} - B_2 = M_X - B_3 \quad (40)$$

where $T_{(CM)} = (2/3)T_N$ is the initial CM kinetic energy of the $N+d$ pair. Therefore, assuming for example $M_X = 17$ MeV, $T_{(CM)}^{min} = M_X - B_3 + B_2 = 10.7$ MeV for $n+d$ and 11.5 MeV for $p+d$. The minimum beam energies in the laboratory system are therefore 16.1 MeV for $n+d$ and 17.3 MeV for $p+d$.

In case of production of an X17, the emission angle between the two leptons is practically determined by the kinematics. For example, let us consider the emission of the two leptons in the plane perpendicular to \mathbf{p} , the momentum of the incident beam, so that $\mathbf{q} \cdot \mathbf{p} = 0$. Disregarding $q^2/2M_3$ in Eq. (38), we have $\omega = \epsilon + \epsilon' \approx E_0$. As discussed above, the X17 is produced when $Q^2 \approx M_X^2$. This condition implies that

$$\cos \theta_{ee} = \frac{m_e^2 + \frac{E_0^2}{4}(1-y^2) - \frac{M_X^2}{2}}{\sqrt{\frac{E_0^2}{4}(1+y)^2 - m_e^2} \sqrt{\frac{E_0^2}{4}(1-y)^2 - m_e^2}} , \quad (41)$$

where

$$y = \frac{\epsilon - \epsilon'}{\epsilon + \epsilon'} . \quad (42)$$

As the lepton energies vary between m_e and $\approx E_0 - m_e$, clearly $-1 < y < +1$. Eq. (41) fixes θ_{ee} in terms of y , E_0 and M_X . For some values of these quantities, one may find that $|\cos \theta_{ee}| > 1$. In such cases, the X17 emission is clearly kinematically forbidden. As an example, we show in Fig. 1 θ_{ee} vs y for $M_X = 17$ MeV and for three different proton beam energies for the reaction $d(p, e^+e^-)^3\text{He}$. As it can be seen, the minimum opening angle between the two leptons (which corresponds to the peak in the angular distribution) moves to lower and lower values as E_0 is increased.

C. Decomposition of the matrix elements

The matrix elements j_{EM}^μ and j_X^c can be decomposed *i*) by expressing the initial scattering wave function Ψ_{m_2, m_1} in components of definite total angular momentum and parity and *ii*) performing a multipolar expansion of the operators (for more details, see Ref. [40]). For the “four-vector” cases j_{EM}^μ and $j_X^{c=V,A}$, we consider the multipolar expansion of the charge, transverse, and lon-

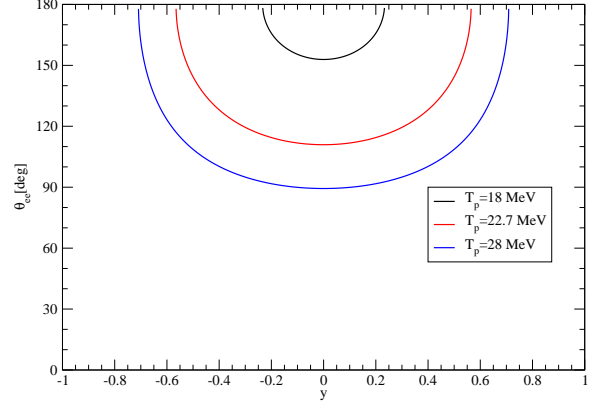


FIG. 1. (color online) The laboratory opening angle θ_{ee} between the two leptons in case of emission of an X17 as function of the quantity y , defined in Eq. (42), for different values of E_0 . The relation between E_0 and T_p is given in Eq. (39). Here we are considering the reaction $d(p, e^+e^-)^3\text{He}$ and $M_X = 17$ MeV.

gitudinal parts:

$$\begin{aligned} \langle \Phi_{m_3} | \rho^\dagger | \Psi_{m_2, m_1} \rangle = & \sum_{\ell m, LSJJ_z} 4\pi(1, m_2, \frac{1}{2}, m_1 | S, J_z) (L, 0, S, J_z | J, J_z) \\ & \times \left(\frac{1}{2}, m_3, J, -J_z | \ell, m \right) \sqrt{2L+1} i^L (-i)^\ell e^{i\sigma_L} \\ & \times (-)^{J-J_z} e^{-im\phi_q} d_{-m, 0}^J(-\theta_q) C_\ell^{LSJ}(q), \end{aligned} \quad (43)$$

$$\begin{aligned} \langle \Phi_{m_3} | \hat{e}_\lambda^* \cdot \mathbf{j}^\dagger(\mathbf{q}) | \Psi_{m_2, m_1} \rangle = & - \sum_{\ell m, LSJJ_z} \sqrt{2\pi^2} (1, m_2, \frac{1}{2}, m_1 | S, J_z) (L, 0, S, J_z | J, J_z) \\ & \times \left(\frac{1}{2}, m_3, J, -J_z | \ell, m \right) \sqrt{2L+1} i^L (-i)^\ell e^{i\sigma_L} \\ & \times (-)^{J-J_z} e^{-im\phi_q} d_{-m, -\lambda}^J(-\theta_q) \\ & \times [\lambda M_\ell^{LSJ}(q) + E_\ell^{LSJ}(q)] , \end{aligned} \quad (44)$$

$$\begin{aligned} \langle \Phi_{m_3} | \hat{e}_z^* \cdot \mathbf{j}^\dagger(\mathbf{q}) | \Psi_{m_2, m_1} \rangle = & \sum_{\ell m, LSJJ_z} 4\pi(1, m_2, \frac{1}{2}, m_1 | S, J_z) (L, 0, S, J_z | J, J_z) \\ & \times \left(\frac{1}{2}, m_3, J, -J_z | \ell, m \right) \sqrt{2L+1} i^L (-i)^\ell e^{i\sigma_L} \\ & \times (-)^{J-J_z} e^{-im\phi_q} d_{-m, 0}^J(-\theta_q) L_\ell^{LSJ}(q) , \end{aligned} \quad (45)$$

where $\lambda = \pm 1$, and C_ℓ^{LSJ} , E_ℓ^{LSJ} , M_ℓ^{LSJ} , and L_ℓ^{LSJ} denote the reduced matrix elements (RMEs) of the charge (C), transverse electric (E), transverse magnetic (M), and longitudinal (L) multipole operators, defined as in Ref. [60]. Above, σ_L is the Coulomb phase shift and we have introduced the basis of unit vectors

$$\hat{e}_z = \hat{q} , \quad \hat{e}_y = \frac{\mathbf{p} \times \mathbf{q}}{|\mathbf{p} \times \mathbf{q}|} , \quad \hat{e}_x = \hat{e}_y \times \hat{e}_z , \quad (46)$$

and $\mathbf{e}_\pm = \mp(\hat{e}_x \pm i \hat{e}_y)/\sqrt{2}$. Clearly, for the cases $c = S$ and P , only the charge matrix elements of Eq. (43)

are needed. Moreover, in the EM case, using current conservation, it is possible to write the matrix elements of the longitudinal component of the current operator in terms of those of the charge operator.

In the matrix elements above, the spin quantization axis of the nuclear states is taken along the incident nucleon momentum $\mathbf{p} = p \hat{\mathbf{z}}$ rather than the three-momentum transfer $\mathbf{q} = q \hat{\mathbf{e}}_z$, as usual. For this reason, we needed to introduce Wigner rotation matrices $d_{M',M}^J$ [61]. The angles θ_q and ϕ_q specify the direction of \mathbf{q} in the lab frame (with \mathbf{p} along $\hat{\mathbf{z}}$). Finally, the RMEs are computed in a frame where \mathbf{q} is along z , where $d_{M',M}^J(0) = \delta_{M',M}$.

D. The cross section for $d(p, e^+ e^-)^3\text{He}$ and $d(n, e^+ e^-)^3\text{H}$ processes

The general expression of the five-fold differential cross section can be schematically written as

$$\begin{aligned} \frac{d^5\sigma}{d\epsilon d\hat{\mathbf{k}} d\hat{\mathbf{k}}'} &= \frac{2}{3(2\pi)^3} \frac{\alpha^2}{v} k k' f_{\text{rec}} \left[\frac{R_{EM}(\epsilon, \hat{\mathbf{k}}, \hat{\mathbf{k}}')}{Q^4} \right. \\ &+ \frac{\varepsilon_e^c R_X(\epsilon, \hat{\mathbf{k}}, \hat{\mathbf{k}}')}{Q^2 D_X} + c.c. + \frac{(\varepsilon_e^c)^2 R_{XX}(\epsilon, \hat{\mathbf{k}}, \hat{\mathbf{k}}')}{|D_X|^2} \left. \right], \\ &= \frac{2}{3(2\pi)^3} \frac{\alpha^2}{v} k k' f_{\text{rec}} \left[\frac{R_{EM}(\epsilon, \hat{\mathbf{k}}, \hat{\mathbf{k}}')}{Q^4} \right. \\ &+ \frac{\varepsilon_e^c R_X(\epsilon, \hat{\mathbf{k}}, \hat{\mathbf{k}}') D_X^* / Q^2 + c.c.}{|D_X|^2} \\ &\left. + \frac{(\varepsilon_e^c)^2 R_{XX}(\epsilon, \hat{\mathbf{k}}, \hat{\mathbf{k}}')}{|D_X|^2} \right], \end{aligned} \quad (47)$$

where v is the $N+d$ relative velocity, $D_X = Q^2 - M_X^2$ (we remember that $Q^2 = q^\mu q_\mu$) and the three terms denote the contributions coming solely from EM currents, the interference between EM and X17-induced currents, and purely X17-induced currents, respectively. The positron energy ϵ' is fixed by energy conservation. In the laboratory coordinate system, where the z -axis is oriented along the incident beam momentum \mathbf{p} , the spherical angles specifying the $\hat{\mathbf{k}}$ ($\hat{\mathbf{k}}'$) direction are denoted as θ and ϕ (θ' and ϕ'), and

$$\hat{\mathbf{k}} \cdot \hat{\mathbf{k}}' \equiv \cos \theta_{ee} = \cos \theta \cos \theta' + \sin \theta \sin \theta' \cos(\phi' - \phi). \quad (48)$$

In Eq. (47) we have made explicit the dependence on the X17-electron coupling constant ε_e^c . The quantity R_X (R_{XX}) depends linearly (quadratically) on the X17-hadron coupling constants $\eta_{0,z}^c$. Finally, the recoil factor is

$$f_{\text{rec}}^{-1} = \left| 1 + \frac{1}{M_3} (k' - p \cos \theta' + k \cos \theta_{ee}) \frac{\epsilon'}{k'} \right|, \quad (49)$$

where θ' is the angle between the directions of the positron and incident nucleon momenta, and θ_{ee} is the

angle between the momenta of the two leptons defined in Eq. (48).

The quantities R_{EM} , R_X , and R_{XX} can be obtained as combinations of the matrix elements given in Eqs. (43)–(45) and kinematical terms depending on the leptonic variables. For example,

$$R_{EM} = \sum_{n=1}^6 v_n R_n, \quad (50)$$

where

$$\begin{aligned} v_1 &= (Q^4/q^4)(\epsilon \epsilon' + \mathbf{k} \cdot \mathbf{k}' - m_e^2), \\ v_2 &= -P_x [\epsilon - \epsilon' - (\omega/q) P_z]/\sqrt{2}, \\ v_3 &= -P_y [\epsilon - \epsilon' - (\omega/q) P_z]/\sqrt{2}, \\ v_4 &= -(P_x^2 + P_y^2)/4 + m_e^2 + \epsilon \epsilon' - \mathbf{k} \cdot \mathbf{k}', \\ v_5 &= (P_x^2 - P_y^2)/2, \\ v_6 &= -P_x P_y, \end{aligned} \quad (51)$$

and

$$\begin{aligned} R_1 &= \sum_{m_3, m_1} |\rho_{fi}|^2, \\ R_2 &= \sum_{m_3, m_1} \text{Re} [\rho_{fi}^* (j_{fi}^+ - j_{fi}^-)], \\ R_3 &= \sum_{m_3, m_1} \text{Im} [\rho_{fi}^* (j_{fi}^+ + j_{fi}^-)], \\ R_4 &= \sum_{m_3, m_1} (|j_{fi}^+|^2 + |j_{fi}^-|^2), \\ R_5 &= \sum_{m_3, m_1} \text{Re} (j_{fi}^{+*} j_{fi}^-), \\ R_6 &= \sum_{m_3, m_1} \text{Im} (j_{fi}^{+*} j_{fi}^-). \end{aligned} \quad (52)$$

Above ρ_{fi} and j_{fi}^\pm are the matrix elements given in Eqs. (43) and (44), respectively, while P_a denotes the component of $\mathbf{P} = \mathbf{k} - \mathbf{k}'$ along \mathbf{e}_a . The expressions for R_X and R_{XX} are explicitly given in Ref. [40].

The four-fold differential cross section is obtained by integrating over the electron energy,

$$\frac{d^4\sigma}{d\hat{\mathbf{k}} d\hat{\mathbf{k}}'} = \int_{m_e}^{\epsilon_{\text{max}}} d\epsilon \frac{d^5\sigma}{d\epsilon d\hat{\mathbf{k}} d\hat{\mathbf{k}}'}, \quad (53)$$

where the maximum allowed energy ϵ_{max} is obtained from the solution of Eq. (37) for the case of a vanishing positron momentum; in fact, since the kinetic energy of the recoiling trinucleon bound state is tiny, ϵ_{max} is close to $E_0 - m_e$.

To account for the decay of X17, we introduce a width Γ_X and will make in Eq. (47) the replacement

$$M_X \longrightarrow M_X - i \Gamma_X/2. \quad (54)$$

Hence, $D_X = Q^2 - M_X^2 + \frac{\Gamma_X^2}{4} + i M_X \Gamma_X$. Assuming that the predominant decay channel of X17 is in $e^+ e^-$ [11],

then

$$\Gamma_X \sim \alpha (\varepsilon_e^c)^2 M_X . \quad (55)$$

Given the current bounds on ε_e^c ($\sim 10^{-3}$ as discussed in Sec. I), we have $\Gamma_X \ll M_X$ and $D_X \approx Q^2 - M_X^2 + iM_X\Gamma_X$. Now, the X17 contribution to the cross section (the two terms $\sim 1/|D_X|^2$) is only sizeable where $Q^2 - M_X^2 = 0$ [40]. We can distinguish two kinematical regions of ϵ , $\hat{\mathbf{k}}$, and $\hat{\mathbf{k}}'$ values:

- Region A, where the $Q^2 - M_X^2 = 0$ is never satisfied; in that region, the contribution of the X17 is always negligible with respect to the EM one, therefore here we can safely assume that

$$\frac{d^5\sigma}{d\epsilon d\hat{\mathbf{k}} d\hat{\mathbf{k}}'} = \frac{2}{3(2\pi)^3} \frac{\alpha^2}{v} k k' f_{\text{rec}} \frac{R_{EM}(\epsilon, \hat{\mathbf{k}}, \hat{\mathbf{k}}')}{Q^4} . \quad (56)$$

- Region B, where $Q^2 - M_X^2 = 0$ is satisfied for some values of ϵ , $\hat{\mathbf{k}}$, and $\hat{\mathbf{k}}'$. For fixed values of $\hat{\mathbf{k}}$, and $\hat{\mathbf{k}}'$, the condition $Q^2 - M_X^2 = 0$ is verified for two values of ϵ , denoted in the following as ϵ_i , $i = 1, 2$ [40]; since Γ_X is very small, $1/|D_X|^2$ is always negligible except for $\epsilon \approx \epsilon_i$, where it assumes the form of a very narrow Lorentzian, which can be very well represented by a delta function; namely,

$$\frac{1}{|D_X|^2} \rightarrow \sum_{i=1,2} \frac{\gamma_i}{(\varepsilon_e^c)^2} \delta(\epsilon - \epsilon_i) , \quad (57)$$

where γ_i are factors independent on ϵ and ε_e^c [40] (clearly, ϵ_i and γ_i depend on the given choice of $\hat{\mathbf{k}}, \hat{\mathbf{k}}'$). Above, we have taken into account the dependence of Γ_X on ε_e^c given in Eq. (55). It is worthwhile to point out that, in region B, the interference contribution (proportional to R_X) is always negligible relative to the R_{XX} term [40]. Therefore, we can write

$$\begin{aligned} \frac{d^5\sigma}{d\epsilon d\hat{\mathbf{k}} d\hat{\mathbf{k}}'} &= \frac{2}{3(2\pi)^3} \frac{\alpha^2}{v} k k' f_{\text{rec}} \left[\frac{R_{EM}(\epsilon, \hat{\mathbf{k}}, \hat{\mathbf{k}}')}{Q^4} \right. \\ &\quad \left. + \sum_{i=1,2} R_{XX}(\epsilon_i, \hat{\mathbf{k}}, \hat{\mathbf{k}}') \gamma_i \delta(\epsilon - \epsilon_i) \right] . \quad (58) \end{aligned}$$

Note that, in the present tree-level treatment of the X17 width, the cross-section becomes independent on ε_e^c .

In order to obtain the four-fold differential cross section, the integration over ϵ is carried out numerically for the EM term, and analytically for the term with R_{XX} (if present). In next section, we will mostly present the calculated four-fold differential cross sections for the leptons emitted in the perpendicular plane with respect to the incident nucleon momentum (i.e. for $\theta = \theta' = 90$ deg) and vs. θ_{ee} . In some cases, we also present the results for other values of θ and θ' . We account roughly for a (possible) finite angular resolution of the detector employed in

an eventual future experiment by folding the θ_{ee} dependence of this (four-fold) cross section with a normalized Gaussian of width Δ , chosen to be $\Delta = 2.5$ deg. This folding has practically no effect on the EM part, as the dependence on θ_{ee} in this case is rather flat, but it is effective to smooth out the peak due to the exchange of the X17, see Ref. [40] for more details.

Finally, we will report also the results for the total cross sections of the $d(p, \gamma)^3\text{He}$ and $d(n, \gamma)^3\text{H}$ radiative captures. They are given by

$$\sigma_C = \frac{16\pi^2\alpha}{3v} \frac{q}{1+q/M_3} \sum_{\ell LS, J \geq 1} \left[|E_\ell^{LSJ}(q)|^2 + |M_\ell^{LSJ}(q)|^2 \right] , \quad (59)$$

where q is the momentum of the outgoing photon and the sum only includes EM transverse RMEs.

III. RESULTS

We list in Table I the RMEs contributing to the transition from an initial $^{2S+1}L_J$ 2+1 scattering state to the final trinucleon ground state with $J^\pi = \frac{1}{2}^+$. Note that the multipolarity ℓ of the RME has to be in the range $|J - \frac{1}{2}| \leq \ell \leq J + \frac{1}{2}$.

TABLE I. The RMEs C_ℓ^{LSJ} , E_ℓ^{LSJ} , M_ℓ^{LSJ} , and L_ℓ^{LSJ} contributing to the EM and X17 transitions from an initial 2+1 $^{2S+1}L_J$ scattering state to the final trinucleon ground state.

state	EM,S,V cases			
	$^{2S+1}L_J$	C_ℓ^{LSJ}	E_ℓ^{LSJ}	M_ℓ^{LSJ}
$\frac{1}{2}^+$	$^2S_{\frac{1}{2}}, ^4D_{\frac{1}{2}}$	$C_0^{LS\frac{1}{2}}$	—	$M_1^{LS\frac{1}{2}}$
$\frac{1}{2}^-$	$^2P_{\frac{1}{2}}, ^4P_{\frac{1}{2}}$	$C_1^{LS\frac{1}{2}}$	$E_1^{LS\frac{1}{2}}$	—
$\frac{3}{2}^+$	$^4S_{\frac{3}{2}}, ^2D_{\frac{3}{2}}, ^4D_{\frac{3}{2}}$	$C_2^{LS\frac{3}{2}}$	$M_1^{LS\frac{3}{2}}$	$E_2^{LS\frac{3}{2}}$
$\frac{3}{2}^-$	$^2P_{\frac{3}{2}}, ^4P_{\frac{3}{2}}, ^4F_{\frac{3}{2}}$	$C_1^{LS\frac{3}{2}}$	$M_2^{LS\frac{3}{2}}$	$E_1^{LS\frac{3}{2}}$
$\frac{5}{2}^+$	$^2D_{\frac{5}{2}}, ^4D_{\frac{5}{2}}, ^4G_{\frac{5}{2}}$	$C_2^{LS\frac{5}{2}}$	$M_3^{LS\frac{5}{2}}$	$E_2^{LS\frac{5}{2}}$
$\frac{5}{2}^-$	$^4P_{\frac{5}{2}}, ^2F_{\frac{5}{2}}, ^4F_{\frac{5}{2}}$	$C_3^{LS\frac{5}{2}}$	$M_2^{LS\frac{5}{2}}$	$E_3^{LS\frac{5}{2}}$

state	P,A cases			
	$^{2S+1}L_J$	C_ℓ^{LSJ}	E_ℓ^{LSJ}	M_ℓ^{LSJ}
$\frac{1}{2}^+$	$^2S_{\frac{1}{2}}, ^4D_{\frac{1}{2}}$	$C_1^{LS\frac{1}{2}}$	$E_1^{LS\frac{1}{2}}$	—
$\frac{1}{2}^-$	$^2P_{\frac{1}{2}}, ^4P_{\frac{1}{2}}$	$C_0^{LS\frac{1}{2}}$	—	$M_1^{LS\frac{1}{2}}$
$\frac{3}{2}^+$	$^4S_{\frac{3}{2}}, ^2D_{\frac{3}{2}}, ^4D_{\frac{3}{2}}$	$C_1^{LS\frac{3}{2}}$	$M_2^{LS\frac{3}{2}}$	$E_1^{LS\frac{3}{2}}$
$\frac{3}{2}^-$	$^2P_{\frac{3}{2}}, ^4P_{\frac{3}{2}}, ^4F_{\frac{3}{2}}$	$C_2^{LS\frac{3}{2}}$	$M_1^{LS\frac{3}{2}}$	$E_2^{LS\frac{3}{2}}$
$\frac{5}{2}^+$	$^2D_{\frac{5}{2}}, ^4D_{\frac{5}{2}}, ^4G_{\frac{5}{2}}$	$C_3^{LS\frac{5}{2}}$	$M_2^{LS\frac{5}{2}}$	$E_3^{LS\frac{5}{2}}$
$\frac{5}{2}^-$	$^4P_{\frac{5}{2}}, ^2F_{\frac{5}{2}}, ^4F_{\frac{5}{2}}$	$C_2^{LS\frac{5}{2}}$	$M_3^{LS\frac{5}{2}}$	$E_2^{LS\frac{5}{2}}$

A. Results for the electromagnetic IPC

In the EM case, the long-wavelength approximation (of relevance here) relates the electric and Coulomb operators, respectively $\hat{E}_{JM}(q)$ and $\hat{C}_{JM}(q)$, via [60]

$$\hat{E}_{JM}(q) \approx \sqrt{\frac{J+1}{J}} \frac{\Delta E}{q} \hat{C}_{JM}(q), \quad (60)$$

where $\Delta E = E_i - E_f$ is the difference between the initial $2+1$ scattering state and trinucleon ground state energies (Siegert's theorem [62]). This relation implies a relationship between the corresponding EM RMEs $E_{\ell}^{LSJ}(q)$ and $C_{\ell}^{LSJ}(q)$. It is worthwhile stressing here that Siegert's theorem assumes (i) a conserved current and (ii) that the initial and final states are exact eigenstates of the nuclear Hamiltonian. Eq. (60) provides a test—indeed, a rather stringent one—of these two assumptions, see Ref. [53] for a discussion of this issue in the context of the chiral interaction NVIA and accompanying EM currents.

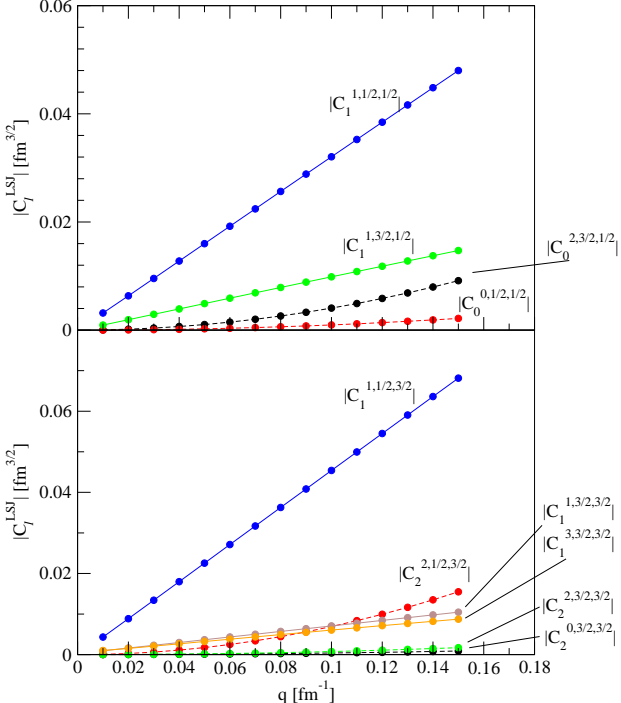


FIG. 2. (color online) The dependence on the three-momentum transfer q of some charge EM RMEs (solid circles); the calculations are at incident proton energy of 18 MeV and use the AV18UIX interaction. The solid (dashed) lines show fits of the calculated values using linear (quadratic) parametrizations. Smaller RMEs are not shown.

We report in Figs. 2 and 3 the EM RMEs calculated with the AV18UIX interaction for $p+d$ at $T_p = 18$ MeV. From the figures, we can see that the largest RMEs are the C_1 's and E_1 's coming from the transitions $\frac{1}{2}^- \rightarrow \frac{1}{2}^+$ and $\frac{3}{2}^- \rightarrow \frac{1}{2}^+$. In fact, in this range of energies we are in the region of the giant dipole resonance, hence the

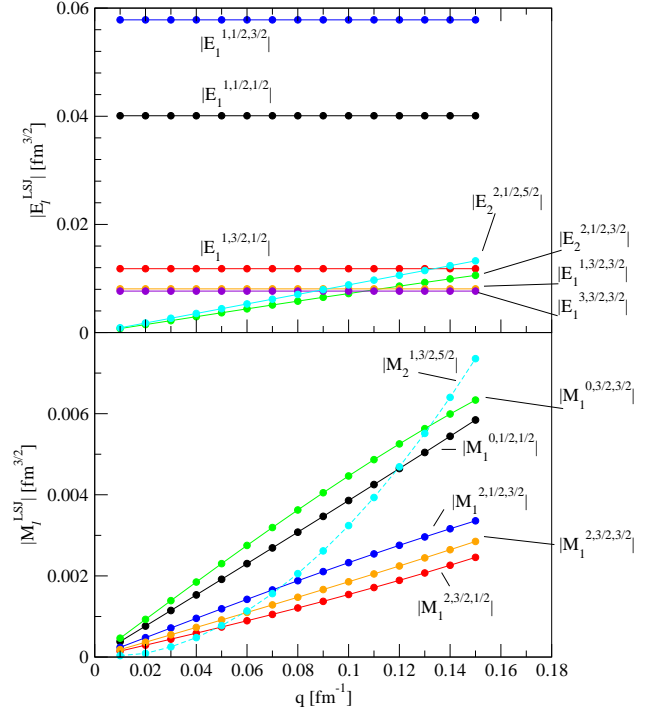


FIG. 3. (color online) The same as in Fig. 2 but for the electric and magnetic EM RMEs.

importance of the E_1 transitions. To understand the q dependence of this transition, we recall that C_1 RME involves the matrix element of the operator proportional to $\sum_i \frac{1}{2} (1 + \tau_z(i)) j_1(qr_i)$, where j_1 is a spherical Bessel function of order 1. Therefore, at small q , we deduce that these $C_1 \sim q$. From Eq. (60), then we obtain that $E_1 \sim q^0$. We note also that $|E_1^{1,\frac{1}{2},J}| > |E_1^{1,\frac{3}{2},J}|$ for both $J = \frac{1}{2}$ and $\frac{3}{2}$. This is related to the fact that the E_1 operator is essentially spin-independent. As a consequence, such an operator can connect the large S -wave component having total spin $S = \frac{1}{2}$ in the trinucleon ground states to the 2P_J scattering state. However, this does not happen for the 4P_J scattering state because of orthogonality between the spin states. Consequently, the transitions from the 4P_J scattering states proceed only via the small components of the trinucleon ground state (these components account for roughly 8% of the trinucleon normalizations).

The transition $\frac{1}{2}^+ \rightarrow \frac{1}{2}^+$ is suppressed for two reasons. At these energies, the $N-d$ interaction in this wave is repulsive or only slightly attractive. Moreover, at LO $C_0^{L,S,\frac{1}{2}}$ involves the matrix element of the \hat{C}_0 multipole operator proportional to $\sum_i \frac{1}{2} (1 + \tau_z(i)) j_0(qr_i)$ between the $N+d$ scattering and trinucleon ground state wave functions. In the q expansion of the spherical Bessel function, the “leading” term is $\sum_i \frac{1}{2} (1 + \tau_z(i)) = \frac{3}{2} + \hat{T}_z$, where \hat{T}_z is the z -component of the total isospin operator. Since $\hat{T}_z |N+d\rangle = \pm \frac{1}{2}$, then this leading term

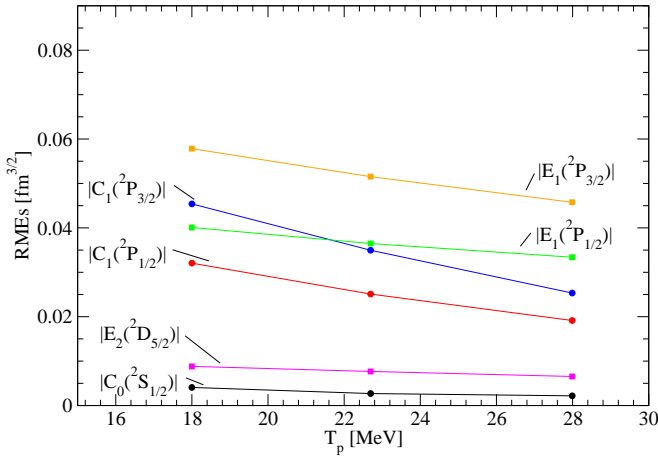


FIG. 4. (color online) The dependence on the proton incident energy T_p of some EM RMEs (solid symbols); the calculations are at a fixed three-momentum transfer $q = 0.1 \text{ fm}^{-1}$ and use the AV18UIX interaction. The lines are to guide the eyes only.

gives a vanishing contribution to the matrix element because of the orthogonality between the ground and scattering states, and hence the $C_0^{L,S,\frac{1}{2}}$ RME is proportional to q^2 . We note that at these energies, it is even found that $|C_0^{2,\frac{3}{2},\frac{1}{2}}| > |C_0^{0,\frac{1}{2},\frac{1}{2}}|$.

Regarding the transition $\frac{3}{2}^+ \rightarrow \frac{1}{2}^+$, the contribution of the ${}^4S_{\frac{3}{2}}$ wave is suppressed since the Pauli principle forbids identical nucleons with parallel spins to come close to each other. In fact, the RME $C_2^{0,\frac{3}{2},\frac{3}{2}}$ is rather suppressed even with respect to $C_2^{2,\frac{1}{2},\frac{3}{2}}$.

Higher-order transitions with $\ell \geq 2$ are usually suppressed by powers of the three-momentum transfer q which is $\lesssim 0.1 \text{ fm}^{-1}$, the only exception being the E_2 transition involving the ${}^2D_{\frac{5}{2}}$ channel, this case being favoured by the fact that the Pauli principle does not play any role, and the scattering state being a $S = \frac{1}{2}$ state. We note finally that all the magnetic RMEs result to be rather small.

Figure 4 shows the behavior of selected $p+d$ EM RMEs (the largest ones) as function of the incident proton energy. As it can be seen, the behaviour of these (and also of the others) RMEs is monotonically decreasing, reflecting the absence of resonances in the trinucleon spectrum.

Let us compare now the $p+d$ and $n+d$ RMEs. In Table II, we report a selected set of RMEs calculated for both reactions for a beam energy of 18 MeV. As it can be seen, the largest E_1 RMEs are almost identical (due to the fact that the C_1 are related to the E_1 , the same is observed for these RMEs). This can be understood since the E_1 operator is essentially an isovector, therefore $E_1^{LSJ}(p+d) \approx -E_1^{LSJ}(n+d)$. For other RMEs, usually the $p+d$ are larger (often approximately by a factor 2) than those for $n+d$, as one could naively expect since the $p+d$ reactions involves two protons. However, since the

E_1 and C_1 RMEs coming from the transitions $\frac{1}{2}^- \rightarrow \frac{1}{2}^+$ and $\frac{3}{2}^- \rightarrow \frac{1}{2}^+$ are dominant, from this result one can expect that the IPC cross section be approximately the same.

TABLE II. A selected set of RMEs in absolute value (in $\text{fm}^{3/2}$) corresponding to the $p+d$ and $n+d$ reactions, obtained with the AV18UIX and NVIa3N interactions and accompanying EM charge and current operators. The incident nucleon energy is 18 MeV and the three-momentum transfer q is 0.1 fm^{-1} .

RMEs $\times 10^3$	wave	AV18UIX		NVIa3N	
		$p+d$	$n+d$	$p+d$	$n+d$
$ C_0^{0,\frac{1}{2},\frac{1}{2}} $	${}^2S_{\frac{1}{2}}$	4.11	2.12	4.12	2.16
$ C_0^{2,\frac{3}{2},\frac{1}{2}} $	${}^2S_{\frac{1}{2}}$	0.97	0.30	0.99	0.30
$ E_1^{1,\frac{1}{2},\frac{1}{2}} $	${}^2P_{\frac{1}{2}}$	39.36	40.20	40.42	40.32
$ E_1^{1,\frac{3}{2},\frac{1}{2}} $	${}^4P_{\frac{1}{2}}$	12.07	12.45	12.00	12.48
$ E_1^{1,\frac{1}{2},\frac{3}{2}} $	${}^2P_{\frac{3}{2}}$	57.43	57.96	58.36	58.07
$ E_1^{1,\frac{3}{2},\frac{3}{2}} $	${}^4P_{\frac{3}{2}}$	8.02	8.66	8.04	8.64
$ E_2^{2,\frac{1}{2},\frac{5}{2}} $	${}^2D_{\frac{5}{2}}$	8.79	1.92	8.81	1.91
$ M_2^{1,\frac{3}{2},\frac{5}{2}} $	${}^4P_{\frac{5}{2}}$	3.20	2.18	3.25	2.18

Finally, we calculate the cross-sections obtained for the internal pair conversion processes. The calculations use fully converged bound- and scattering-state wave functions (with the largest allowed number of HH states) and the complete N4LO set of EM charge and current operators.

In Fig. 5 we show the $d(p, e^- e^+)^3\text{He}$ and $d(n, e^- e^+)^3\text{H}$ four-fold differential cross sections calculated with the AV18UIX interaction, corresponding to the kinematical configuration in which the lepton pair is emitted in the plane perpendicular to the incident nucleon momentum ($\theta = \theta' = 90^\circ$) and as function of the relative angle θ_{ee} , that is, the angle between the electron and positron momenta. As it can be seen, at each energy, the two cross sections essentially overlap, a result we have anticipated. The cross section has the typical form for an IPC process dominated by the E_1 transition, i.e. it decreases monotonically as θ_{ee} increases, becoming almost flat as $\theta_{ee} \rightarrow 180^\circ$ deg. The small differences between the $p+d$ and $n+d$ results are due mainly to the different value of E_0 , namely the energy at disposal for the two leptons. In fact, in the $n+d$ process, there is the formation of a more bound trinucleon system (${}^3\text{H}$). Hence, the $d(n, e^- e^+)^3\text{H}$ cross section is slightly greater than that of $d(p, e^- e^+)^3\text{He}$. The results obtained with the NVIa3N interaction are very similar to those shown in Fig. 5, in practice the curves obtained with both interactions (and corresponding set of EM transition operators) essentially overlap.

Total cross sections for the processes $d(p, e^- e^+)^3\text{He}$, $d(p, \gamma)^3\text{He}$, $d(n, e^- e^+)^3\text{H}$, and $d(n, \gamma)^3\text{H}$, calculated at a

TABLE III. Total cross sections (in μb) for the processes $d(p, e^- e^+)^3\text{He}$, $d(p, \gamma)^3\text{He}$, $d(n, e^- e^+)^3\text{H}$, and $d(n, \gamma)^3\text{H}$ calculated at a number of incident nucleon energies T_N (in MeV) with the AV18UIX and NVIa3N Hamiltonians.

T_N	AV18UIX				NVIa3N			
	$d(p, e^- e^+)^3\text{He}$	$d(p, \gamma)^3\text{He}$	$d(n, e^- e^+)^3\text{H}$	$d(n, \gamma)^3\text{H}$	$d(p, e^- e^+)^3\text{He}$	$d(p, \gamma)^3\text{He}$	$d(n, e^- e^+)^3\text{H}$	$d(n, \gamma)^3\text{H}$
18.0	0.0175	9.06	0.0192	9.55	0.0182	9.39	0.0194	9.59
22.7	0.0165	8.05	0.0178	8.35	0.0170	8.23	0.0177	8.29
28.0	0.0151	7.02	0.0159	7.11	0.0154	7.18	0.0161	7.19

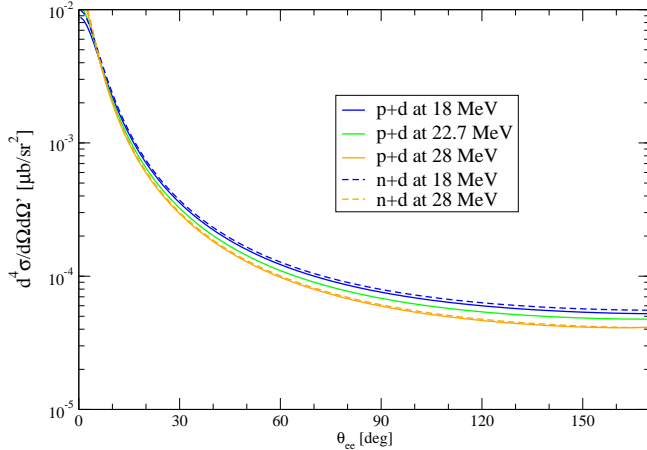


FIG. 5. (color online) The EM-only four-fold differential cross section for the $d(p, e^- e^+)^3\text{He}$ and $d(n, e^- e^+)^3\text{H}$ processes calculated at different incident nucleon energies with the AV18UIX interaction (and accompanying EM currents); the kinematical configuration corresponds to the lepton pair being emitted in the plane perpendicular to the nucleon incident momentum, and θ_{ee} is the angle between the electron and positron momenta. The cross sections for the $d(p, e^- e^+)^3\text{He}$ ($d(n, e^- e^+)^3\text{H}$) processes are shown as solid (dashed) lines. The results for the NVIa3N interaction in practice overlap with those reported in the figure.

number of incident nucleon energies T_N (in MeV) with the AV18UIX and NVIa3N Hamiltonians (and accompanying currents) are reported in Table III. We note that pair production cross sections are suppressed by a factor of approximately 500 relative to radiative capture cross sections. As expected, the difference between the $p + d$ and $n + d$ cross sections is small.

B. Results including the X17 boson

Here we discuss the RMEs derived from the operators given in Eqs. (25)–(30). The q dependence of the RMEs for either the S or V cases are similar to the behaviour already discussed for the EM current. However, now we can analyze the behaviour of the RMEs originating from purely isoscalar and isovector operators. To be definite, we consider the RMEs calculated for the $p + d$ process at $T_p = 18$ MeV with the AV18UIX interaction.

Let us consider first the S case. The corresponding charge RMEs calculated using the operators given in Eq. (25) are shown in Fig. 6. As it can be seen, in case of the transitions $\frac{1}{2}^- \rightarrow \frac{1}{2}^+$ and $\frac{3}{2}^- \rightarrow \frac{1}{2}^+$, the $C_1^{1,S,J,+}$ RMEs are dramatically suppressed. It is easy to show that they behave as q^3 . In fact, they are calculated from the matrix elements

$$\langle ^3\text{He} | \sum_{j=1,3} e^{i\mathbf{q} \cdot \mathbf{r}_j^{(CM)}} | pd, {}^{2S+1}P_J \rangle , \quad (61)$$

where $\mathbf{r}_j^{(CM)}$ above is the distance of particle j to the CM of the three particle system (the dependence on the CM position R_{CM} has been integrated out to obtain the momentum conservation). Expanding the plane wave, the even powers of $(i\mathbf{q} \cdot \mathbf{r}_j^{(CM)})$ vanish due to the parity constraint. The linear term in $i\mathbf{q} \cdot \mathbf{r}_j^{(CM)}$ also vanishes since in the integral

$$\langle ^3\text{He} | \sum_{j=1,3} i\mathbf{q} \cdot \mathbf{r}_j^{(CM)} | pd, {}^{2S+1}P_J \rangle , \quad (62)$$

we have $\sum_j \mathbf{r}_j^{(CM)} = 0$ by definition. The first nonvanishing term is therefore proportional to q^3 . Since in our case q is small, the corresponding RMEs are suppressed. We note that the “ $\lambda = -$ ” RMEs come from the matrix element of the operator given in Eq. (25)

$$\langle ^3\text{He} | \sum_{j=1,3} e^{i\mathbf{q} \cdot \mathbf{r}_j^{(CM)}} \tau_{j,3} | pd, {}^{2S+1}P_J \rangle , \quad (63)$$

and consequently the first nonvanishing contribution is the linear one, proportional to q .

In case of a vector X17, the charge RMEs derive from the same operators given in Eq. (25). Regarding the transverse and longitudinal RMEs, we need to consider the operators given in Eqs. (28) and (29). Some of the electric RMEs given by the operator of Eq. (28) are shown in Fig. 7. Again, the “ $\lambda = +$ ” components are sup-

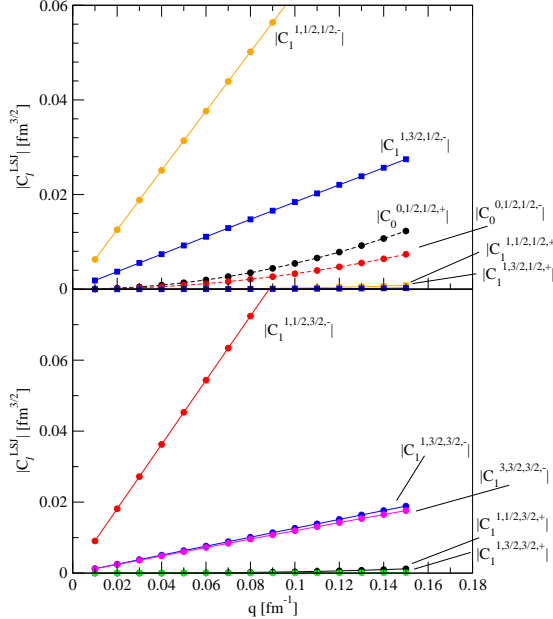


FIG. 6. (color online) The dependence on the three-momentum transfer q of some RMEs for the charge operators given in Eq. (25); the calculations are at incident proton energy of 18 MeV and use the AV18UIX interaction. The solid, dashed, an dotted lines show fits of the calculated values using linear, quadratic, and cubic parametrizations, respectively. The RMEs not shown in this plot are negligible.

pressed, since this isoscalar operator can be written as

$$\begin{aligned}
 j^{V+}(q) &= \frac{1}{2m_N} \sum_j \left[e^{i\mathbf{q} \cdot \mathbf{r}_j^{(CM)}}, \mathbf{p}_j \right]_+, \\
 &\approx \frac{1}{2m_N} \sum_j \left[\left(1 + \frac{1}{2} (i\mathbf{q} \cdot \mathbf{r}_j^{(CM)})^2 \right), \mathbf{p}_j \right]_+, \\
 &= \frac{1}{2m_N} \left\{ 2\mathbf{P} \right. \\
 &\quad \left. + \sum_j \left[\frac{1}{2} (i\mathbf{q} \cdot \mathbf{r}_j^{(CM)})^2, \mathbf{p}_j \right]_+ \right\}, \quad (64)
 \end{aligned}$$

where $\mathbf{P} = \sum_i \mathbf{p}_i$. The matrix element between the nuclear states is then proportional to q^2 , since $\mathbf{P}|pd, {}^{2S+1}P_J\rangle = 0$ (the ket contains the CM wave function). On the other hand, the same argument does not apply to the “ $\lambda = -$ ” component, due to the presence of the operator $\tau_{i,3}$ in the sum over the particles. In fact the “ $\lambda = -$ ” RMEs are independent on q , and therefore are much larger than the “ $\lambda = +$ ” RMEs.

In the V current, we have added also the contribution of the operator given in Eq. (29). In this case, the contribution of the “ $\lambda = +$ ” and “ $\lambda = -$ ” components are of the same order of magnitude. However, this contribution is much less than the contribution of j^V , and therefore this term does not change the situation. This is confirmed by the calculations, reported in Fig. 7. The longitudinal RMEs behave similarly, while the magnetic

RMEs are always very small.

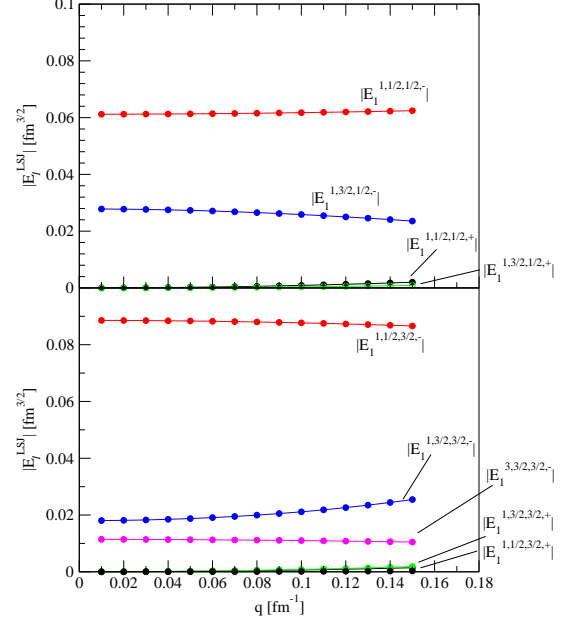


FIG. 7. (color online) The same as Fig. 6 but for the electric RMEs coming from Eq. (28).

The q dependence of the RMEs coming from the P and A operators reported in Eq. (26), (27), and (30) are shown in Figs. 8, 9, and 10. Note that the RMEs associated with the pseudoscalar and the time component of the axial operators behave differently. In these cases, there is no suppression of the “ $\lambda = +$ ” component.

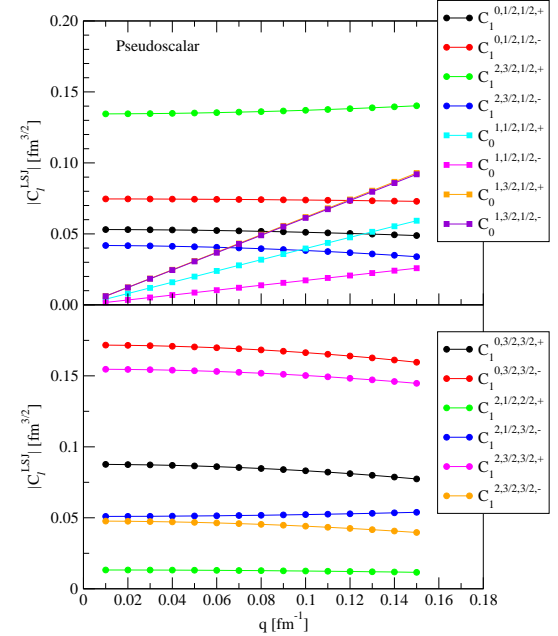


FIG. 8. (color online) Same as Fig. 6 but for the charge RMEs derived from the pseudoscalar operator given in Eq. (26).

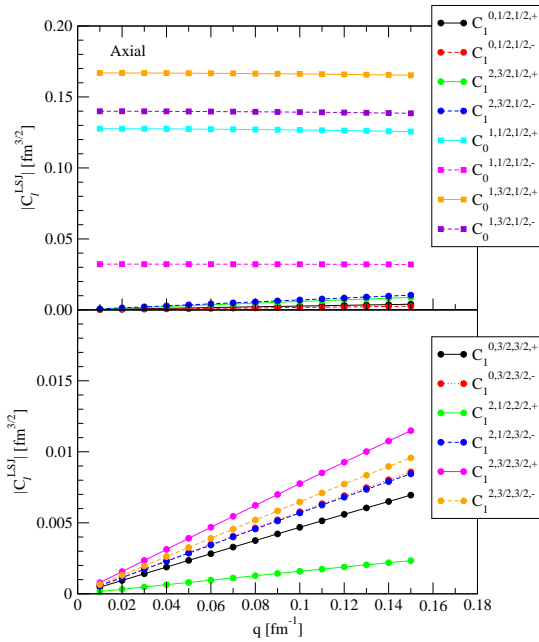


FIG. 9. (color online) Same as in Fig. 6 but for the charge RMEs derived from the axial operator given in Eq. (28).

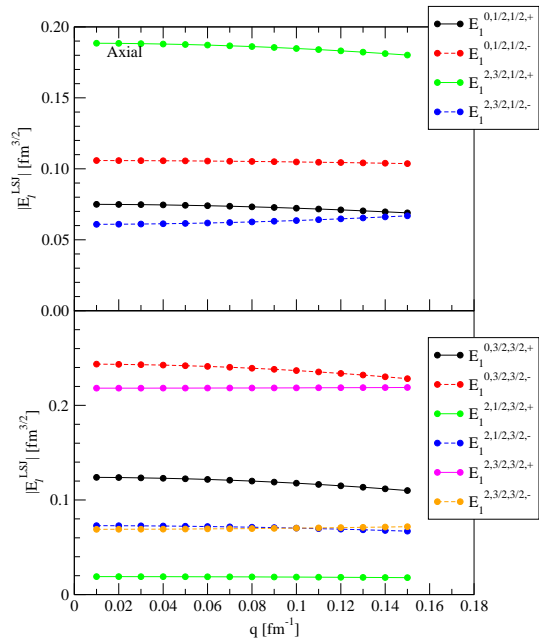


FIG. 10. (color online) Same as in Fig. 6 but for the electric RMEs derived from the axial operator given in Eq. (30).

Regarding the energy dependence, in all cases the RMEs smoothly decrease as the energy is increased, similar to what found for the EM RMEs.

The absolute values of a selected set of RMEs (generally the largest ones), calculated for the $n + d$ and $p + d$ processes, are compared in Table IV. For the S and V cases, we report the dominating C_1 and E_1 RMEs, com-

ing from the transitions $\frac{1}{2}^- \rightarrow \frac{1}{2}^+$ and $\frac{3}{2}^- \rightarrow \frac{1}{2}^+$. As it can be seen, the difference between the $p + d$ and $n + d$ absolute values of these RMEs are rather tiny. We note again that the RMEs originating from the “ $\lambda = +$ ” operators are much smaller than those calculated from the “ $\lambda = -$ ” operators. On the other hand, for the P and A cases, there is no particular difference between the “ $\lambda = +$ ” and “ $\lambda = -$ ” RMEs. Regarding the effective values of the $p + d$ and $n + d$ RMEs (not the absolute values), generally the “ $\lambda = +$ ” RMEs have the same sign, while the “ $\lambda = -$ ” have different sign.

TABLE IV. A selected set of RMEs in absolute value (in $\text{fm}^{3/2}$) corresponding to the $p + d$ and $n + d$ reactions, obtained with the AV18UIX interaction and the operators given in Eqs. (25)–(30). The incident nucleon energy is 18 MeV and the three-momentum transfer q is 0.1 fm^{-1} .

S case					
RMEs $\times 10^3$	wave	$p + d$	$n + d$	$\lambda = +$	$\lambda = -$
$ C_1^{1,\frac{1}{2},\frac{1}{2},\lambda} $	$^2P_{\frac{1}{2}}$	0.22	62.2	0.19	61.0
$ C_1^{1,\frac{1}{2},\frac{3}{2},\lambda} $	$^2P_{\frac{3}{2}}$	0.33	90.9	0.29	88.0
V case					
RMEs $\times 10^3$	wave	$p + d$	$n + d$	$\lambda = +$	$\lambda = -$
$ E_1^{1,\frac{1}{2},\frac{1}{2},\lambda} $	$^2P_{\frac{1}{2}}$	0.90	61.7	0.87	61.8
$ E_1^{1,\frac{3}{2},\frac{1}{2},\lambda} $	$^4P_{\frac{1}{2}}$	0.40	25.8	0.40	26.9
$ E_1^{1,\frac{1}{2},\frac{3}{2},\lambda} $	$^2P_{\frac{3}{2}}$	0.64	87.7	0.62	87.8
$ E_1^{1,\frac{3}{2},\frac{3}{2},\lambda} $	$^4P_{\frac{3}{2}}$	0.82	21.1	0.82	21.8
P case					
RMEs $\times 10^3$	wave	$p + d$	$n + d$	$\lambda = +$	$\lambda = -$
$ C_1^{0,\frac{1}{2},\frac{1}{2},\lambda} $	$^2S_{\frac{1}{2}}$	51.1	73.8	50.4	69.6
$ C_1^{0,\frac{3}{2},\frac{3}{2},\lambda} $	$^4S_{\frac{3}{2}}$	83.1	166.3	83.2	156.9
A case					
RMEs $\times 10^3$	wave	$p + d$	$n + d$	$\lambda = +$	$\lambda = -$
$ C_0^{1,\frac{1}{2},\frac{1}{2},\lambda} $	$^2P_{\frac{1}{2}}$	127.7	32.1	127.1	33.4
$ C_0^{1,\frac{3}{2},\frac{1}{2},\lambda} $	$^4P_{\frac{1}{2}}$	166.2	139.3	168.9	140.1
$ E_1^{0,\frac{1}{2},\frac{1}{2},\lambda} $	$^2S_{\frac{1}{2}}$	72.2	104.8	71.2	98.7
$ E_1^{0,\frac{3}{2},\frac{3}{2},\lambda} $	$^4S_{\frac{3}{2}}$	117.7	236.8	117.9	223.3

Let us now present the results of the four-fold cross section for the processes $d(p, e^+e^-)^3\text{He}$ and $d(n, e^+e^-)^3\text{H}$. The cross sections have been calculated assuming the values for ε_0^c and ε_z^c given in Table V. These values were obtained in Ref. [40] by reproducing the 2019 ATOMKI data for the process $^3\text{H}(p, e^+e^-)^4\text{He}$, using the same NVIA3N interaction employed here. However, as discussed in that paper, such extraction is rather uncertain, due to the quality of those experimental data (lack of

subtraction of the leptonic pairs produced by real gammas hitting the apparatus, etc.). So these values have to be considered only as indicative. Anyway, we will use them in this paper to have an idea of the eventual X17 effects in the $A = 3$ system.

TABLE V. Values of the coupling constants ε_0^c and ε_z^c , $c = S, P, V, A$, obtained in Ref. [40] from the fit of the ${}^3\text{H}(p, e^+ e^-) {}^4\text{He}$ 2019 ATOMKI angular distribution [2] at $T_p = 0.90$ MeV. In all cases, one of the coupling constant has been fixed to a given value (evidentiated in bold), while the other has been chosen in order to reproduce the ATOMKI data. In the V case, the adopted choice corresponds to a proto-phobic X17. See Ref. [40] for more details.

NVIA3N		
Case c	ε_0^c	ε_z^c
S	0.75×10^0	0
P	2.72×10^1	0
V	2.66×10^{-3}	$-3 \varepsilon_0^V$
A	2.89×10^{-3}	0

Once clarified this point, the $d(p, e^+ e^-) {}^3\text{He}$ four-fold cross sections calculated with NVIA3N at various energies are reported in Fig. 11, for the emission of the lepton in the laboratory plane perpendicular to the incident beam momentum ($\theta = \theta' = 90$ deg), and as function of the angle θ_{ee} . Several comments are in order. (i) The X17 peak moves to lower values of θ_{ee} as the energy increases, as already discussed in Sec. II B. Note the correspondence between the minimum angles where the X17 signal appears shown in Fig. 1 and the position of the peaks in Fig. 11. (ii) For the scalar case, the X17 contribution is very tiny, and the cross section almost coincident with the EM cross section only. This is due to the fact that for the ${}^3\text{H}(p, e^+ e^-) {}^3\text{He}$ process at $T_p = 0.90$ MeV we are rather close to a $0^+ {}^4\text{He}$ resonance, and therefore the X17 RMEs in this case are large, and the adopted value of ε_0^S sufficiently small to reproduce the observed peak. In the present case, however, the RMEs induced by the S operators are small, and therefore the peak is almost unobservable. (iii) For the pseudoscalar case, the peak becomes more and more evident as the beam energy increases. In the case under study ($\varepsilon_0^P \neq 0$ and $\varepsilon_z^P = 0$), the transition operator is proportional to q , whose value q_{peak} at the peak increases as E_0 increases. In fact, for the $d(p, e^+ e^-) {}^3\text{He}$ we have $q_{\text{peak}} = 4.1, 11.7$, and 17.2 MeV/c for $T_p = 18, 22.7$, and 28 MeV, respectively. This explains the rise of the peak in this case. (iv) The height of the peaks with respect to the EM-only cross section due to the vector X17 (at $T_p = 22.7$ and 28 MeV) is approximately constant with energy. This is related to the fact that the operators inducing the X17 in this case are practically the same as those appearing in the EM current. (v) The peaks at $T_p = 18$ MeV are a bit at variance with respect to the other two energies, but this may be due to the smallness of the phase space in this case.

So although the three nucleon spectrum has not any structure, it can be exploited to distinguish between the various cases. (i) No observation of the signal with respect to the signal observed in ${}^3\text{H}(p, e^+ e^-) {}^3\text{He}$ would be explained by a scalar X17; (ii) a constant height of the peak when the beam energy is increased would indicate the presence of a vector X17; (iii) an increase of the peak height with the beam energy would point out to a pseudoscalar X17; (iv) the vector and axial cases could in principle be distinguished by looking at the angular dependence of the cross section: as $\theta_{ee} \rightarrow 180$ deg, the cross section decays faster in the A case than in the V case.

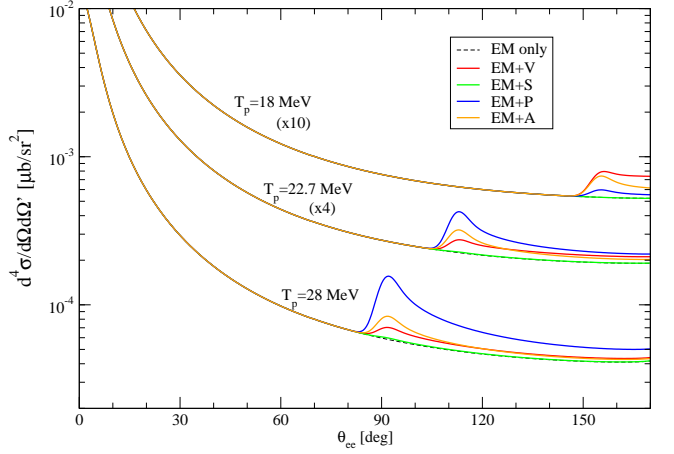


FIG. 11. (color online) The $d(p, e^+ e^-) {}^3\text{He}$ four-fold cross sections calculated with the NVIA3N interaction as function of the angle θ_{ee} at various energies. Here $\theta = \theta' = 90$ deg. The EM-only cross section (dashed lines) is compared with those obtained by including the effect of the exchange of an X17, for the S , P , V , and A cases. The used quark-X17 coupling constants are given in Table V. The EM+S curve is always almost coincident to the EM curve. Note that the cross sections calculated at $T_p = 18$ MeV (22.7 MeV) have been rescaled by a factor 10 (4) for the sake of clarity. As discussed at the end of Sec. II, the cross section has been folded with a normalized Gaussian of width $\Delta = 2.5$ deg, in order to approximately take into account of experimental finite angular resolution of the detectors.

Clearly, a greater amount of information can be obtained by detecting the leptons out of the perpendicular plane. As an example, we report in Fig. 12 the $d(p, e^+ e^-) {}^3\text{He}$ four-fold cross section calculated with NVIA3N at $T_p = 22.7$ MeV, for four different values of the polar angles $\theta = \theta'$ (chosen to be equal). The cross section is calculated as function of $\Delta\phi = \phi - \phi'$ (the azimuthal angles of the two leptons). For the P case, we observe a noticeable increase of the height of the peak as $\theta = \theta'$ decrease. This happens since at $\theta = \theta' = 90$ deg the X17 contribution for this case is kinematically suppressed. Then, out of the perpendicular plane, where the kinematical suppression is less and less effective, the X17 contribution for the P case starts to become larger and larger. For the V and A cases, the X17 contribution is approximately the same as $\theta = \theta'$ decrease. How-

ever, it is possible to note that the peak for the A case becomes smaller than the peak for the V case as the lepton polar angles become smaller and smaller. Finally, for $\theta = \theta' = 60$ deg, the X17 contribution for the S case starts to become visible, although it remains rather small. Therefore, from this example, we see that the X17 peak varies differently for the S , P , V , and A cases as the polar angles are varied, giving better handles to learn about the X17 spin and parity.

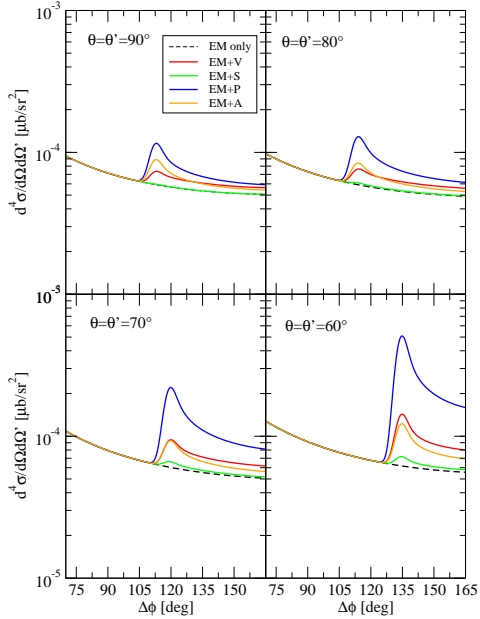


FIG. 12. (color online) The $d(p, e^+e^-)^3\text{He}$ four-fold cross sections calculated with the NVIa3N interaction at $T_p = 22.7$ MeV and for different values of θ and θ' (but retaining $\theta = \theta'$), the angles of the momenta of the two leptons with respect to the z axis (the z axis is chosen to be along the direction of the incident beam). The cross sections are reported as function of the angle $\Delta\phi = \phi - \phi'$ (the azimuthal angles of the two leptons). For the notation, see Fig. 11.

C. The cross section for the $p+d$ and $n+d$ processes

In this subsection, we investigate the difference of the X17 signal in the two processes $d(p, e^+e^-)^3\text{He}$ and $d(n, e^+e^-)^3\text{H}$. Since in the second process the number of neutrons is twice than in the first process, from the (eventual) measurements of both cross sections, one could extract information about the isospin dependence of the X17-nucleon interaction, namely the relative magnitude of the coupling constants ε_0^c and ε_z^c . In particular, one could test the proto-phobic X17 hypothesis which, as discussed in the Sec. I, was formulated for a vector X17 in order to avoid the constraint of the NA48 limit. Hereafter we will not consider the scalar case, as we have seen that the eventual X17 signal is expected to be very tiny in these two reactions.

Let us first consider the case of a vector X17. The cross sections for the $d(p, e^+e^-)^3\text{He}$ and $d(n, e^+e^-)^3\text{H}$ processes calculated at $T_N = 28$ MeV for a proto-phobic X17, i.e. with the coupling constants satisfying the condition of Eq. (12), are shown in Fig. 13. As it can be seen, in this case, the heights of the two peaks are comparable (for the $n+d$ process, the phase space is slightly larger and the peak starts at lower values of θ_{ee} , both effects due to the larger E_0).

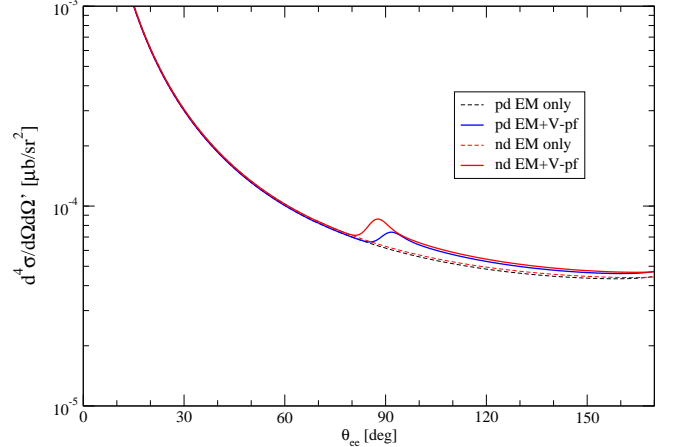


FIG. 13. (color online) The $d(p, e^+e^-)^3\text{He}$ and $d(n, e^+e^-)^3\text{H}$ four-fold cross sections calculated with the NVIa3N interaction in function of the angle θ_{ee} at a beam energy of 28 MeV and for $\theta = \theta' = 90$ deg. The cross sections for the two processes in case of a proto-phobic vector X17 (curves labeled EM+V-pf) are shown, and compared with those obtained for the EM-only case. As in Fig. 11, the cross section has been folded with a normalized Gaussian of width $\Delta = 2.5$ deg.

The vector current with the choice of Eq. (12) reads at LO

$$j_V = e \sum_i \varepsilon_0^V \frac{1 - \tau_{i,3}}{2} e^{i\mathbf{q} \cdot \mathbf{r}_i^{(CM)}} + \dots \quad (65)$$

Now, for this case and in this range of energies, the largest RMEs are the E_1 RMEs, coming from the transitions $\frac{1}{2}^- \rightarrow \frac{1}{2}^+$ and $\frac{3}{2}^- \rightarrow \frac{1}{2}^+$. As we have already discussed in the previous subsection, however, the isoscalar part of the operator in Eq. (65) gives vanishing contributions with respect to the isovector part, and consequently $j_V|n+d\rangle \approx -j_V|p+d\rangle$. So the effect of a greater number of neutrons in the $d(n, e^+e^-)^3\text{H}$ process is not effective in this case.

In the vector current we have also considered the part proportional to $\boldsymbol{\sigma} \times \mathbf{q}$. Both isoscalar and isovector contributions are of the same order for this operator. However, the contribution to the RMEs coming from this term is rather small, and therefore does not help. Further contributions at NLO come from one-pion-exchange diagrams, which however give isovector operators. Clearly, matrix elements of these operators are of the same order of magnitude in the two processes. Therefore, also these

contributions will likely not give substantial differences between the $p + d$ and $n + d$ processes. .

Let us consider the axial case. The dominant contribution comes from the spatial part, which in our LO approximation reads

$$j_A = e \sum_i \left[(3F - D)\varepsilon_0^A + (F + D)\varepsilon_z^A \tau_{i,3} \right] \sigma_i e^{i\mathbf{q} \cdot \mathbf{r}_i^{(CM)}}. \quad (66)$$

Let us choose a proto-phobic X17, namely so that $(3F - D)\varepsilon_0^A + (F + D)\varepsilon_z^A = 0$. The cross sections for the $d(p, e^+e^-)^3\text{He}$ and $d(n, e^+e^-)^3\text{H}$ processes calculated at $T_N = 28$ MeV in this case are shown in Fig. 14. As it can be seen, the peak for the $n + d$ process is almost twice higher than for the $p + d$ case. As we have seen in Sec. III B, in this case both the isoscalar and isovector RMEs are of the same order of magnitude. Therefore, the $n + d$ cross section turns out to be larger than for the $p + d$ process.

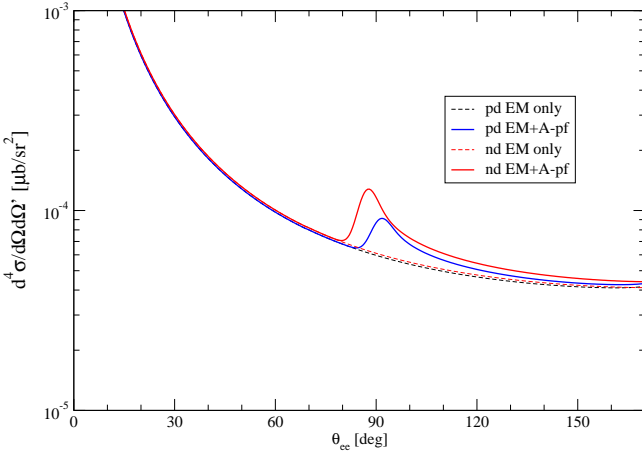


FIG. 14. (color online) The same as in Fig.13 but for a proto-phobic axial X17 (curves labeled EM+A-pf).

Finally, let us comment about the pseudoscalar case. As discussed in Sec. III B, the isoscalar and isovector operator have different origin: the isoscalar comes from the direct coupling of X17 to the nucleon, coming by terms in the N2LO Lagrangian and proportional to the LECs $d_{18} + 2d_{19}$. The isovector operator comes from the direct coupling of the X17 to the neutral pion. Therefore, it would be rather strange that the different coupling would be fine-tuned to create a proto-phobic interaction. According to the model of Refs. [19, 20], the direct pion-X17 is suppressed. Therefore, we have (at the chiral order considered in this paper) only an isoscalar interaction. Considering this latter case, the cross sections for the $d(p, e^+e^-)^3\text{He}$ and $d(n, e^+e^-)^3\text{H}$ processes calculated at $T_N = 28$ MeV with NVIa3N are shown in Fig. 15. As it can be seen, the two cross sections have similar magnitude, as expected for an interaction which does not distinguish between protons and neutrons. The slightly larger $n + d$ cross section is related to the phase space (larger value of E_0).

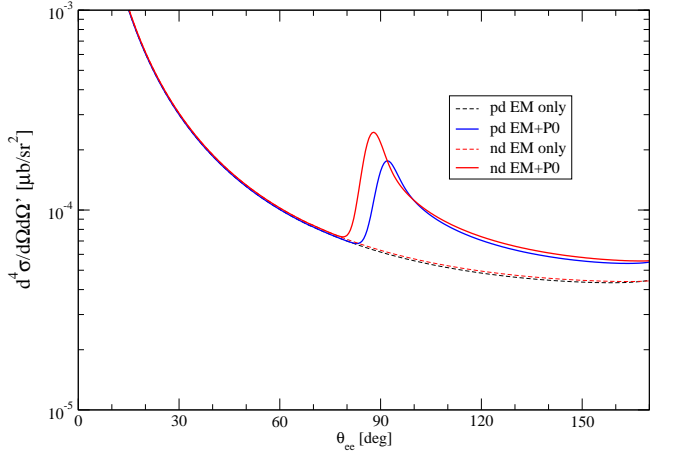


FIG. 15. (color online) The same as in Fig.13 but for a isoscalar pseudoscalar X17 (curves labeled EM+P0).

IV. CONCLUSIONS

In this paper, we have studied the e^+e^- pair production in the $d(p, e^+e^-)^3\text{He}$ and $d(n, e^+e^-)^3\text{H}$ processes, in order to evidenitiate possible effects due to the exchange of a hypothetical low-mass boson, the so-called X17. These processes are studied for energies of the incident beams in the range 18-30 MeV, in order to have a sufficient energy to produce such a boson, whose mass is estimated to be around 17 MeV. We have first analyzed the reactions as a purely electromagnetic processes, in the context of a state-of-the-art approach to nuclear strong-interaction dynamics and nuclear electromagnetic currents, the latter derived from χ EFT. The initial $2 + 1$ scattering-state and trinucleon bound-state wave functions have been obtained using the HH method. Therefore, the comparison with accurate data for the cross sections of these processes could be already very useful (also in case of no observation of the X17), being a stringent test of our current knowledge of the strong and EM interactions in nuclear systems.

Next, we have investigated how the exchange of a hypothetical low-mass boson would impact the cross sections for such processes. We have considered several possibilities, that this boson be either a scalar, pseudoscalar, vector, or axial particle. The $A = 3$ system does not present any excited-state structure, however the study of the cross section and the eventual observation of a peak in the e^+e^- angular distribution could be very instructive. First of all, the experiment appears to be well feasible, since a deuteron target is easily manageable. Varying the energy of the incident beam, under a certain threshold no peak should be observed, then the variation of the position of the peak with increasing energy would give important constraints on the mass of the X17. The variation of the height of the peak with energy would be also very instructive on the nature of X17. Finally, the comparison of the $d(p, e^+e^-)^3\text{He}$ and $d(n, e^+e^-)^3\text{H}$ cross

sections could give information on the coupling of X17 with protons and neutrons separately. Although there is not much sensitivity to verify the alleged proto-phobicity in the case of a vector or pseudoscalar X17, in the axial case the peak for the $n + d$ process is almost twice higher than in the $p + d$ case. More information about the nature of X17 and its couplings with protons and neutrons can be achieved by detecting the leptons in the full 4π space. In this paper, we have limit ourselves to study the case of emission at identical polar angles $\theta = \theta'$, but a more complete study is in progress.

Therefore, from the experimental point of view, a detector designed to probe the existence and properties of X17 should have a large angular acceptance. Another critical property is that it should have a low sensitivity to the neutrons produced by the deuterium spallation, that otherwise can represent a severe background to

the observation of the subdominant ${}^2\text{H}(\text{p},\text{X17}){}^3\text{He}$ and ${}^2\text{H}(\text{n},\text{X17}){}^3\text{H}$ decay channels. In fact, to produce the X17, the beam energies have to be chosen to be well above the threshold of the deuterium disintegration.

Finally, here the X17-nucleon interaction has been considered only at LO (with inclusion of some NLO contributions) for the sake of simplicity. However, the present treatment can be extended to include higher order contributions in the framework of χ EFT, as well. Work in this direction is in progress.

ACKNOWLEDGMENTS

We gratefully acknowledge Rocco Schiavilla for useful discussions and the support of the INFN-Pisa computing center.

[1] A. J. Krasznahorkay *et al.*, Phys. Rev. Lett. **116**, 042501 (2016), arXiv:1504.01527 [nucl-ex].

[2] A. Krasznahorkay *et al.*, (2019), arXiv:1910.10459 [nucl-ex].

[3] A. J. Krasznahorkay, M. Csatlós, L. Csige, J. Gulyás, A. Krasznahorkay, B. M. Nyakó, I. Rajta, J. Timár, I. Vajda, and N. J. Sas, Phys. Rev. C **104**, 044003 (2021), arXiv:2104.10075 [nucl-ex].

[4] N. J. Sas *et al.*, (2022), arXiv:2205.07744 [nucl-ex].

[5] A. J. Krasznahorkay *et al.*, Phys. Rev. C **106**, L061601 (2022), arXiv:2209.10795 [nucl-ex].

[6] T. T. Anh *et al.*, Universe **10**, 168 (2024), arXiv:2401.11676 [nucl-ex].

[7] M. Battaglieri *et al.*, in *U.S. Cosmic Visions: New Ideas in Dark Matter* (2017) arXiv:1707.04591 [hep-ph].

[8] M. Pospelov, A. Ritz, and M. Voloshin, Physics Letters B **662**, 53 (2008).

[9] D. Banerjee *et al.* (NA64), Phys. Rev. Lett. **120**, 231802 (2018), arXiv:1803.07748 [hep-ex].

[10] J. Batley *et al.* (NA48/2), Phys. Lett. B **746**, 178 (2015), arXiv:1504.00607 [hep-ex].

[11] J. L. Feng, B. Fornal, I. Galon, S. Gardner, J. Smolinsky, T. M. P. Tait, and P. Tanedo, Phys. Rev. Lett. **117**, 071803 (2016), arXiv:1604.07411 [hep-ph].

[12] X. Zhang and G. A. Miller, Phys. Lett. B **773**, 159 (2017), arXiv:1703.04588 [nucl-th].

[13] U. Ellwanger and S. Moretti, J. High Energ. Phys. **2016**, 39 (2016), arXiv:1609.01669 [hep-ph].

[14] B. Fornal, Int. J. Mod. Phys. A **32**, 1730020 (2017), arXiv:1707.09749 [hep-ph].

[15] J. A. Dror, R. Lasenby, and M. Pospelov, Phys. Rev. Lett. **119**, 141803 (2017), arXiv:1705.06726 [hep-ph].

[16] L. Delle Rose, S. Khalil, and S. Moretti, Phys. Rev. D **96**, 115024 (2017), arXiv:1704.03436 [hep-ph].

[17] L. Delle Rose, S. Khalil, S. J. King, S. Moretti, and A. M. Thabt, Phys. Rev. D **99**, 055022 (2019), arXiv:1811.07953 [hep-ph].

[18] L. Delle Rose, S. Khalil, S. J. King, and S. Moretti, Front. in Phys. **7**, 73 (2019), arXiv:1812.05497 [hep-ph].

[19] D. S. M. Alves and N. Weiner, JHEP **07**, 092 (2018), arXiv:1710.03764 [hep-ph].

[20] D. S. M. Alves, Phys. Rev. D **103**, 055018 (2021), arXiv:2009.05578 [hep-ph].

[21] J. Bordes, H.-M. Chan, and S. T. Tsou, Int. J. Mod. Phys. A **34**, 1950140 (2019), arXiv:1906.09229 [hep-ph].

[22] C. H. Nam, Eur. Phys. J. C **80**, 231 (2020), arXiv:1907.09819 [hep-ph].

[23] D. Kirpichnikov, V. E. Lyubovitskij, and A. S. Zhevlakov, Phys. Rev. D **102**, 095024 (2020), arXiv:2002.07496 [hep-ph].

[24] P. Fayet, Physical Review D **103**, 035034 (2021), arXiv:2010.04673 [hep-ph].

[25] A. C. Hayes, J. L. Friar, G. Hale, and G. Garvey, (2021), arXiv:2106.06834 [nucl-th].

[26] C.-Y. Wong, in *Shedding light on X17* (2022) arXiv:2201.09764 [hep-ph].

[27] D. Barducci and C. Toni, JHEP **02**, 154 (2023), [Erratum: JHEP 07, 168 (2023)], arXiv:2212.06453 [hep-ph].

[28] M. Hostert and M. Pospelov, Phys. Rev. D **108**, 055011 (2023), arXiv:2306.15077 [hep-ph].

[29] A. M. Baldini *et al.* (MEG II), Eur. Phys. J. C **78**, 380 (2018), arXiv:1801.04688 [physics.ins-det].

[30] J. Bialecki *et al.* (2014) arXiv:1412.4717 [physics.ins-det].

[31] C. Ahn *et al.* (SHiP), (2020), arXiv:2010.11057 [hep-ex].

[32] t. P. G. Azuelos, in *New Scientific Opportunities at the TRIUMF ARIEL e-linac*.

[33] t. P. B.H. Dongwi, in *New Scientific Opportunities at the TRIUMF ARIEL e-linac*.

[34] L. Darmé, M. Mancini, E. Nardi, and M. Raggi, Phys. Rev. D **106**, 115036 (2022), arXiv:2209.09261 [hep-ph].

[35] E. Kou, P. Urquijo, W. Altmannshofer, *et al.* (Belle-II), Prog. Theor. Exp. Phys. **2019**, 123C01 (2019), [Erratum: PTEP 2020, 029201 (2020)], arXiv:1808.10567 [hep-ex].

[36] D. Banerjee, J. Bernhard, V. E. Burtsev, A. G. Chumakov, D. Cooke, P. Crivelli, E. Depero, A. V. Dermenev, S. V. Donskov, R. R. Dusaev, T. Enik, N. Charitonidis, A. Feshchenko, V. N. Frolov, A. Gardikis, S. G. Gerassimov, S. N. Gnninenko, M. Hösgen, M. Jeckel, V. A. Kachanov, A. E. Karneyeu, G. Kekelidze, B. Ketzer, D. V. Kirpichnikov, M. M. Kirsanov, V. N. Kolosov, I. V. Konorov, S. G. Kovalenko, V. A. Kramarenko, L. V. Kravchuk, N. V. Krasnikov, S. V. Kuleshov, V. E. Lyubovitskij, V. Lysan, V. A. Matveev, Y. V. Mikhailov, L. Molina Bueno, D. V. Peshekhonov, V. A. Polyakov, B. Radics, R. Rojas, A. Rubbia, V. D. Samoylenko, D. Shchukin, V. O. Tikhomirov, I. Tlisova, D. A. Tlisov, A. N. Toropin, A. Y. Trifonov, B. I. Vasilishin, G. Vasquez Arenas, P. V. Volkov, V. Y. Volkov, and P. Ulloa (The NA64 Collaboration), Phys. Rev. D **101**, 071101 (2020).

[37] E. Cisbani, N. Colonna, P. Finocchiaro, S. Fiore, G. Gervino, C. Gustavino, C. Massimi, P. Mastinu, A. Mazzone, F. Renga, and M. Viviani, <https://cds.cern.ch/record/2766541> (2021).

[38] E. Abouzaid *et al.* (KTeV), Phys. Rev. D **75**, 012004 (2007), arXiv:hep-ex/0610072.

[39] S. Egli *et al.* (SINDRUM), Phys. Lett. B **222**, 533 (1989).

[40] M. Viviani, E. Filandri, L. Girlanda, C. Gustavino, A. Kievsky, L. E. Marcucci, and R. Schiavilla, Phys. Rev. C **105**, 014001 (2022), arXiv:2104.07808 [nucl-th].

[41] P. Gysbers, P. Navratil, K. Kravvaris, G. Hupin, and S. Quaglioni, Phys. Rev. C **110**, 015503 (2024), arXiv:2308.13751 [nucl-th].

[42] A. Kievsky, S. Rosati, M. Viviani, L. Marcucci, and L. Girlanda, J. Phys. G **35**, 063101 (2008), arXiv:0805.4688 [nucl-th].

[43] L. E. Marcucci, J. Dohet-Eraly, L. Girlanda, A. Gnech, A. Kievsky, and M. Viviani, Front. in Phys. **8**, 69 (2020), arXiv:1912.09751 [nucl-th].

[44] R. B. Wiringa, V. G. J. Stoks, and R. Schiavilla, Phys. Rev. C **51**, 38 (1995), arXiv:nucl-th/9408016.

[45] B. S. Pudliner, V. R. Pandharipande, J. Carlson, and R. B. Wiringa, Phys. Rev. Lett. **74**, 4396 (1995), arXiv:nucl-th/9502031.

[46] M. Piarulli, L. Girlanda, R. Schiavilla, A. Kievsky, A. Lovato, L. E. Marcucci, S. C. Pieper, M. Viviani, and R. B. Wiringa, Phys. Rev. C **94**, 054007 (2016), arXiv:1606.06335 [nucl-th].

[47] M. Piarulli *et al.*, Phys. Rev. Lett. **120**, 052503 (2018), arXiv:1707.02883 [nucl-th].

[48] E. Epelbaum, A. Nogga, W. Gloeckle, H. Kamada, U.-G. Meissner, and H. Witala, Phys. Rev. C **66**, 064001 (2002), arXiv:0208023 [nucl-th].

[49] S. Pastore, R. Schiavilla, and J. L. Goity, Phys. Rev. C **78**, 064002 (2008), arXiv:0810.1941 [nucl-th].

[50] S. Pastore, L. Girlanda, R. Schiavilla, M. Viviani, and R. Wiringa, Phys. Rev. C **80**, 034004 (2009), arXiv:0906.1800 [nucl-th].

[51] S. Pastore, L. Girlanda, R. Schiavilla, and M. Viviani, Phys. Rev. C **84**, 024001 (2011), arXiv:1106.4539 [nucl-th].

[52] M. Piarulli, L. Girlanda, L. E. Marcucci, S. Pastore, R. Schiavilla, and M. Viviani, Phys. Rev. C **87**, 014006 (2013), arXiv:1212.1105 [nucl-th].

[53] R. Schiavilla *et al.*, Phys. Rev. C **99**, 034005 (2019), arXiv:1809.10180 [nucl-th].

[54] S. Andreas, C. Niebuhr, and A. Ringwald, Phys. Rev. D **86**, 095019 (2012).

[55] E. M. Riordan, M. W. Krasny, K. Lang, P. de Barbaro, A. Bodek, S. Dasu, N. Varelas, X. Wang, R. Arnold, D. Benton, P. Bosted, L. Clogher, A. Lung, S. Rock, Z. Szalata, B. W. Filippone, R. C. Walker, J. D. Bjorken, M. Crisler, A. Para, J. Lambert, J. Button-Shafer, B. Debebe, M. Frodyma, R. S. Hicks, G. A. Peterson, and R. Gearhart, Phys. Rev. Lett. **59**, 755 (1987).

[56] A. Anastasi *et al.*, Phys. Lett. B **750**, 633 (2015), arXiv:1509.00740 [hep-ex].

[57] S. Weinberg, Phys. Rev. **166**, 1568 (1968).

[58] J. Gasser and H. Leutwyler, Annals Phys. **158**, 142 (1984).

[59] V. Bernard, N. Kaiser, and U.-G. Meissner, Int. J. Mod. Phys. E **4**, 193 (1995), arXiv:hep-ph/9501384.

[60] J. D. Walecka, *Theoretical Nuclear and Subnuclear Physics* (Oxford University Press, New York, 1995).

[61] A. Edmonds, *Angular Momentum in Quantum Mechanics* (Princeton University Press, Princeton, 1957).

[62] A. J. F. Siegert, Phys. Rev. **52**, 787 (1937).